Low-temperature thermal conductivity of the amorphous superconductor $Fe_xNi_{1-x}Zr_2$

Olivier Alonzo-Proulx

Department of Physics

McGill University

Montreal, Québec

CANADA

September 2005

A thesis submitted to

McGill University in partial

fulfillment of the requirements

for the degree of Master of Science

Your file Votre référence
ISBN: 978-0-494-24599-6
Our file Notre référence
ISBN: 978-0-494-24599-6

Contents

List of Figures

List of Tables

Abstract

Thermal conductivity is a powerful tool to probe the phonon and electron exitations in a solid, especially in superconductors were one can basically tune the respective electronic and phononic contributions by applying a magnetic field below T_c.

After a short review on the concepts of superconductivity, thermal conductivity and amorphous matter, we present a study of the thermal conductivity of an exotic material, the amorphous metallic superconductor $Fe_{0.5}Ni_{0.5}Zr_2$. The results indicate an unexpected dominant electonic contribution to the thermal conductivity across the superconducting transition, in accordance with an inhomogeneous sample composed of a bulk normal phase with inhomogeneous superconducting phases.

Résumé

La conductivité thermique s'avère être un outil puissant pour déterminer les exitations électroniques et phononiques dans un solide, en particulier dans les supraconducteurs où les contributions respectives des électrons et phonons peuvent être modifiés par l'application d'un champ magnétique en dessous de T_c.

Après une brève révision des concepts de la supraconductivité, de la conductivité thermique et de la matière amorphe, nous présentons une étude de la conductivité thermique d'un matériaux exotique, le supraconductor metallique amorphe $Fe_{0.5}Ni_{0.5}Zr_2$. Ces tests indiquent une inattendue contribution dominante des électrons à la conductivité thermique, et ceci à la fois dans la phase normale que dans la phase supraconductrice. Cette observation est attribuée à un échantillon inhomogène composé d'une phase normale dominante et de phases supraconductrices inhomogènes.

Acknowledgments

First and foremost I would like to thank my supervisor Michael Hilke for his constant support throughout the project. Without his help this work would not have been possible, and through the many challenges I have truly learned from his experience. I was fortunate to work on such an interesting subject, and his constant help and enthusiasm were invaluable.

I thank Robert Gagnon and John Smeros for their constant technical help and advice. Their patience, availability and expertise were greatly appreciated and essential to the completion of this project. I also thank Robert and John for their great sense of humour which contributed the relaxed atmosphere in the lab.

I thank all the group and former group members, Sophie Avesques, Alistair Armstrong-Brown, Olivier Landry, Josianne Lefebvre, Jae-Ho Oh and Alexis Gagnon-Morris for their constant help in the lab, for their patience and for the nice atmosphere they brought to the lab. My special thanks goes to Christian Voyer for his friendship and presence: his restless work habits were an inspiration to me and his animated discussions a total pleasure. I also thank Christian and Josianne for their help in programming my fitting routines, and Zaven Altounian for useful discussions.

I thank the Fonds Québéquois sur la Recherche en Nature et Technologie as well as the McGill University Physics Department for financial support.

Finally I would like to thank Maude Parent for her constant support throughout my studies. Without you things would have been quite different, and I infinitely appreciate your love. I also thank my parents José-Luis and France as well as my sister Agnès for their love and support.

Chapter 1

Introduction

The discovery of superconductivity in 1911 by H. Kamerlingh Onnes [1] was the spark that ignited the fascinating field of low temperature physics which is today a major field of scientific research. At low temperatures matter behaves quite unexpectedly, as the basic blocks of matter: electronic and phononic, charge and spin excitations begin to couple, decouple and form exotic quasiparticles. Good examples are the fractional quantum hall effect, where it was seen [2] that in a 2 dimensional electron gas (a very thin $\sim$100 Å quantum well at the junction of two semiconductors) electron charge separates into particles of charge $e/3$, or of course superconductivity, where electrons form large bound pairs, overcoming Coulomb repulsion, because of a phonon-electron interaction.

In particular, superconductivity has triggered enormous interest because of its remarkable *macroscopic* properties: a superconductor, below a critical temperature T_c and critical magnetic field B_c will become a *perfect* conductor and diamagnet. In this thesis, we deal with very exotic types of superconductors: the amorphous $Fe_xNi_{1-x}Zr_2$ alloys. Those superconductors are of the second type, that is they lose their perfect diamagnetism by allowing the penetration of flux tubes or vortices though the material, each carrying a quantum of flux. Now vortices inside a superconductor form a unique system: they are driven by an external current, pinned by impurities or inhomogeneities, and their density is changed with the applied field. In our high purity Fe-Ni-Zr alloys, the mechanisms of flux pinning and vortex motion is quite unique

because of a very low critical current (the lowest known in the literature) above which the vortex core starts to move, and therefore provide an extraodinary testbed for the study of vortex dynamics. In addition, these systems exhibit the peak effect: an anomalous enhancement of the critical current close to the upper critical field, and contributes the richness and diversity of the vortex phases in those systems [3, 4], as seen in this thesis for the $x = 0.5$ alloy.

Furthermore, the $Fe_xNi_{1-x}Zr_2$ alloys are amorphous. That is their atomic structure is specially disordered with no long range order, i.e. liquid-like: they are obtained via the rapid cooling of the liquid state. Because spacial positioning of the atoms is random in amorphous systems, many equilibrium positions are accessible to the atoms, and at low temperatures only the two lowest levels are relevant, so that amorphous systems unfold into two level systems as demonstrated in 1972 by Anderson [5] and Phillips [6]. As a result, amorphous systems have peculiar thermal properties at low temperature, where the phonon thermal conductivity follows a T^2 relation in temperature instead of a T^3 relation. Thermal conductivity is an excellent tool to distinguish the contributions of electrons and phonons to thermal conductivity in superconductors, and measurements seem to indicate a dominant electronic thermal conductivity, *even* in the superconducting state, and is attributable to the presence of a mixed superconducting phases in parallel to a bulk normal phase.

In this thesis we review in chapter 2 the main theories of superconductivity as well as a description of vortex dynamics and the peak effect. In chapter 3 we cover some aspects of thermal conductivity in normal solids and superconductors. In chapter 4 we give a description of the basic properties of amorphous materials as well as their low temperature thermal properties. Chapter 5 is a discussion about the experimental aspects of this work: the fabrication technique of the samples and their basic physical properties as well as the experimental procedures used to perform low temperature thermal conductivity measurements. Finally, in chapter 6 we present our results on the vortex state of $Fe_{0.5}Ni_{0.5}Zr_2$ and thermal conductivity of $Fe_{0.5}Ni_{0.5}Zr_2$ in the normal and superconducting state between 0.3 and 1.5 K, before concluding.

Chapter 2

Superconductivity

2.1 Introduction

In 1913, Dutch physicist Kamerlingh Onnes was awarded the Nobel Prize in Physics "for his investigations on the properties of matter at low temperatures which led, inter alia, to the production of liquid helium". In his words, from his Nobel Prize lecture relating to the low-temperature resistance of mercury,

> the experiment left no doubt that, as far as accuracy of measurement went, the resistance disappeared. At the same time, however, something unexpected occurred. The disappearance did not take place gradually but *abruptly.* From 1/500 the resistance at 4.2 °K drops to a millionth part. At the lowest temperature, 1.5 °K, it could be established that the resistance had become less than a thousand-millionth part of that at normal temperature.
>
> Thus the mercury at 4.2 °K has entered a new state, which, owing to its particular electrical properties, can be called the state of superconductivity.

Onnes, through his study of low temperatures, had discovered superconductivity [1]. The consequences of his research, his heritage, are truly immense as ninety years later, with discoveries such as BSC theory and high temperature superconductors, superconductivity and more generally low temperature physics is a fundamental part of research in condensed matter physics. Richard Feynman, from his famous lecture

about nanotechnology (Plenty of Room at the Bottom, December 1959), said, "I imagine experimental physicists must often look with envy at men like Kamerlingh Onnes, who discovered a field like low temperature, which seems to be bottomless and in which one can go down and down." Indeed. And today we can benefit from some applications of superconductivity, whether it is high field magnets, magnetic resonance imaging, high speed levitating trains or loss-less power lines.

Superconductivity is the vanishing of electrical resistance at a finite temperature called the critical temperature, denoted by T_c. There is no doubt we are dealing with *perfect* conductivity in superconductors. Of course even the more sensitive measuring device has its uncertainty, but the residual resistivity of superconductors is found to be less than $10^{-27}\Omega \cdot \text{cm}$ [7], 18 orders of magnitude less than a very good conductor such as copper, with a resistivity of $10^{-9}\Omega \cdot \text{cm}$. Another illustration of this *perfect* conductivity is by looking at the decay time of the magnetic field created by a persistent current in a superconducting ring. This decay time has been found to be more than 10^5 years, and actually no change in field or current is expected to occur in less than $10^{10^{10}}$ years [8]!

Twenty years following the discovery of Onnes, in 1933, Meissner and Ochsenfeld [9] discovered another fundamental property of superconductors. They found that magnetic fields are *expelled* from superconductors, that they are also *perfect* diamagnets. Perfect conductors do *exclude* fields because of a zero skin depth, but they would tend to trap flux lines *in* into cooling trough T_c. By cooling a superconductor through T_c with an external field $\mathbf{H}$, we find the magnetic induction $\mathbf{B}$=0 inside the superconductor, *i.e.* the magnetic permeability $\mu = 0$ (we consider the relation $\mathbf{B}=\mu\mathbf{H}$, where $\mu < 1$ for a diamagnet and $\mu > 1$ for a paramagnet). The existence of this Meissner effect implied that superconductivity could now be destroyed by a critical magnetic field, H_c, and is the reason of the spectacular levitation of superconductors above magnetic fields.

So superconductivity is characterized not only by its anomalous electrical properties as suggested by its inspired denomination, but also by anomalous magnetic and thermal properties which we will investigate in the following sections. It is a

remarkable new state of matter observable at low temperatures.

2.2 Zero resistance, a microscopic theory

The phenomenon of superconductivity remained a mystery until a systematic microscopic theory was formulated by Bardeen, Cooper and Schrieffer (BCS[1] theory in 1957). Before that, many brilliant minds such as Einstein, Heisenberg, Landau and Bloch, Frenkel, Gorter and Casimir, had tried but failed to find a solution to the mystery, and their theories now belong to the history of science [7]. More successful were the phenomenological theories of the London brothers in 1935 and of Ginsburg and Landau in 1950, which provided a description of the anomalous diamagnetism in superconductors in respectively weak and strong fields.

The BCS theory is rather involved and will not be discussed here. However, using the main results of this theory, we can still explain the perfect conductivity of superconductors.

2.2.1 Cooper pairs

With the discovery of the isotope effect by Maxwell and Reynolds [10, 11] in 1950, which showed that H_c and T_c were proportional to $M^{-1/2}$ for isotopes of the same element, it became clear that the crystal lattice played a role in superconductivity, through some interaction with the electrons. In fact, this interaction mediates an indirect *attraction* between electrons. The physical idea is that as it moves through the lattice, the electron distorts it, attracting neighboring ions to it by Coulomb interaction. The electron thus become surrounded by an excess positive charge, which can in turn *attract* another electron, overcoming the Coulomb repulsion. At high temperature, this process is less possible, since thermal motion of the ions tend to

[1] John Bardeen, Leon Cooper and Robert Schrieffer were awarded the Physics Nobel Prize in 1972 for their theory. John Bardeen is the only man to have received *two* Nobel Prizes in Physics: in 1956 he received his first with Schockley and Brattain for the discovery of the transistor and their research in semiconductors.

"wash out" the cloud of ions around the electrons. We can note also that good conductors such as gold, copper and silver are not superconductors, precisely because being excellent conductors, the interactions of the electrons with the lattice is very weak, such that the attractive electron-electron interaction can never occur.

This can be seen using quantum mechanics, assuming $T = 0$. A crystal then is in zero-point motion because of the uncertainty principle, and this is the ground state of the crystal system. An electron moving through the lattice excites it to a higher energy state, and upon returning to the ground state, energy is radiated in the crystal in the form of a phonon, a quanta of acoustic vibration. The absorption of this phonon by another electron, the phonon exchange, is then responsible for the attraction between the electrons. In superconductors, this attraction leads to the creation of bound pairs, called Cooper pairs after Leon Cooper who showed in 1956 [12] that a weak attraction between electrons in a Fermi sea would lead systematically to a bound state.

Cooper's theorem has beautiful consequences concerning the dimensionality of the phenomenon of superconductivity. Usually in three dimensions, attractive potentials will yield bound states only if the strength of the potential exceeds a certain value. However in two dimensions, an arbitrary weak attraction potential will in all cases give bound states [7]. In superconductors, electron motion in momentum space is constrained to the Fermi surface, since transitions to lower energy states inside the surface are forbidden because of the Pauli exclusion principle, and because of an energy gap (which we will discuss in the next section), transitions into higher energy state are difficult, and therefore the motion is essentially two-dimensional. It is also interesting to note that in the high-T_c cuprates, electron motion is also confined to the layers of copper-oxide planes.

2.2.2 The energy gap

Any bound state has a binding energy associated with it, the energy required to break the bond or to create it. Thus finite energy is expended in order to create the Cooper pairs in a superconductor, and consequently an energy gap $\Delta(T)$ appears in the energy

spectrum of the electrons. Now electrical resistance in solids is a result of collisions of electrons with the crystal lattice or impurities, which implies quantum transitions of the electron system. But such transitions are not always possible because of the forbidden region in energy space, and as a result, the electron system will *not* be excited, it will advance without friction, namely the resistance will be zero.

In superconductors, the electron energy is given by $\epsilon = \sqrt{\xi^2 + \Delta^2}$, where $\xi = p^2/2m^* - E_F$ (p and m^* are respectively the electron momentum and renormalized mass from Fermi liquid theory) is the electron energy in the normal state, which can be zero. Thus the minimal electron energy is Δ (the binding energy of the pair is 2Δ), and electrons in a layer Δ around E_F will form Cooper pairs. In BCS superconductor, the energy gap $\Delta(r)$ is isotropic.

So superconductivity is a direct consequence of an inter-electron interaction. However an electron will be unequally attracted to the other electrons: according to BCS theory, the strongest bond between electrons will occur when the electrons are of opposite spin and momentum due an exchange of phonons. Since in a solid the state of the electrons changes continuously, the sets of Cooper pairs will also change, and we can imagine superconductivity as a peculiar ball of electrons, where the electron dance, changing partners frequently. And this ball is gigantic. Taking the simplest case, we have $E_F = p_F^2/2m$, so that $\delta E = p_F \delta p/m \approx \Delta$, the spread in energy of the superconducting electrons near the Fermi surface. From the uncertainty relation, $\delta p \delta r \approx \hbar$, so that $\delta r \approx \hbar/\delta p \approx \hbar p_F/\Delta m \approx \hbar v_F/\Delta$, where v_F is the Fermi velocity. So the size –the coherence length ξ_0– of the superconducting electrons, the Cooper pair, is of the order of [7]

$$\xi_0 = \frac{\hbar v_F}{\Delta} \approx 10^4 \text{Å}$$

which is much longer than typical interatomic distances!

We can conclude this section with some fundamental results from BCS theory, which can be used to determine whether a superconductor is of the BCS type. It is

found that

$$\begin{aligned} \Delta(0) &= 1.76 k_B T_c \quad \text{and} \\ \frac{\Delta(T)}{\Delta(0)} &= 1.74\sqrt{1-\frac{T}{T_c}}\,. \end{aligned}$$

These results are valid only in the weak-limit coupling, *i.e.* for weak ($\ll 1$) electron phonon interaction, but they are a good approximation in all cases.

2.3 Magnetic properties

2.3.1 The London Equations

In 1935, the brothers Fritz and Heinz London suggested a phenomenological theory explaining the anomalous diamagnetism of superconductors [13]. It can be understood in adapting the well-known quantum mechanical current equation,

$$\mathbf{J}_s = \frac{\imath e\hbar}{2m}\Big[(\nabla\psi)^*\psi - \psi^*\nabla\psi\Big] - \frac{e^2}{mc}\mathbf{A}\psi^*\psi\ ,$$

where $\mathbf{J}_s$ is the supercurrent, ψ the many-body electron wavefunction and $\mathbf{A}$ the vector potential of the field. In the general case, ψ is complex and the left-hand term (called the paramagnetic term) is non-zero. This is due to the "deformability" of ψ versus the field [7], *i.e.* its implicit dependance on it. They assumed however that ψ was "rigid", so that it retained its form with or without a field. This way the paramagnetic term would vanish [7], leaving the London equation

$$\mathbf{J}_s = -\frac{e^2}{mc}|\psi|^2\mathbf{A}. \tag{2.1}$$

There is another way to see this rigidity [8]. Considering the canonical momentum $\mathbf{p} = m\mathbf{v} + e\mathbf{A}/c$ of the electron, and arguing that in the superconducting ground state and without field, the net momentum is zero (because Cooper pairs have equal and opposite momentum), we obtain the net velocity of the electrons in the superconducting state,

$$\langle \mathbf{v}_s \rangle = -\frac{e}{mc}\mathbf{A}.$$

This holds assuming again the ground state is rigid. Thus with n_s the density of superconducting electrons, we obtain

$$\mathbf{J}_s = n_s e\langle \mathbf{v}_s \rangle = -\frac{n_s e^2}{mc}\mathbf{A}, \tag{2.2}$$

which is the same as (2.1) with $|\psi|^2 = n_s$.

Combining (2.2) with the Maxwell equation $\nabla \times \mathbf{H} = 4\pi\mathbf{J}/c$, and taking the curl of both equations, we obtain

$$\nabla^2\mathbf{H} = \frac{4\pi n_s e^2}{mc^2}\mathbf{H},$$

and solving this differential equation with a superconductor for $z > 0$ and vacuum for $z < 0$, we have

$$H(z) = H(0)e^{-z/\lambda_L},$$

where $\lambda_L^2 = \frac{mc^2}{4\pi n_s e^2}$. This implies that a magnetic field is screened from a superconductor, with a characteristic penetration depth λ_L, the Meissner effect.

2.3.2 Pippard's non-local approach

The London equation is *local*. That is the field at each point is determined only by the supercurrent at the *same* point. We don't expect this to hold in superconductors, as the field at an electron site will also affect its pair mate a distance ξ_0 away. Because of the spacial correlation of electrons in superconductors, we need a *non-local* field-current relation.

Pippard [14] proposed such a model in 1953, with a non-local generalization of the London equation, done in analogy to Chambers non-local generalization of Ohm's law [15] $\mathbf{J}(\mathbf{r}) = \sigma\mathbf{E}(\mathbf{r})$, obtained assuming that the current at a point $\mathbf{r}$ depends on $\mathbf{E}(\mathbf{r'})$ within a volume of radius l:

$$\mathbf{J}(\mathbf{r}) = \frac{3\sigma}{4\pi}\int \frac{\mathbf{R}\Big[\mathbf{R}\cdot\mathbf{E}(\mathbf{r'})\Big]e^{-R/l}}{R^4}\mathrm{d}\mathbf{r'},$$

where $\mathbf{R} = \mathbf{r} - \mathbf{r'}$. Pippard, in his work, introduced the coherence length ξ_0 as a characteristic correlation length in the superconducting state, and obtained in a

similar fashion

$$\mathbf{J}_s(\mathbf{r}) = \frac{3c^2}{(4\pi\lambda_L)^2\xi_0}\int \frac{\mathbf{R}\left[\mathbf{R}\cdot\mathbf{A}(\mathbf{r'})\right]e^{-R/\xi_0}}{R^4}\mathrm{d}\mathbf{r'}. \tag{2.3}$$

Pippards equation (2.3) was a real triumph of intuition and general physics, fitting experimental data quite well, while its form was confirmed with the BCS theory. It simplifies to the London equation (2.2) when $\xi_0 \ll \lambda_L$, which holds for lead and indium. However in the case where the field $\mathbf{A}$ varies appreciably on the distance $\xi_0 \gg \lambda_L$, we expect from (2.3) to have a weakened supercurrent response which would compensate the field, thus giving a "real" penetration depth λ, much larger than λ_L. This holds for materials such as tin, aluminum, mercury, which are called Pippard type.

2.3.3 The demagnetization factor

The Meissner effect imposes strict conditions on the magnetic field $\mathbf{B}$ around a superconductor when an external field $\mathbf{H}_a$ is applied, namely that $\mathbf{B}\rightarrow \mu_0\mathbf{H}_a$ when far from the superconducting sample and that $\mathbf{B}$=0 at the superconductor boundary. By studying those boundary conditions for fields outside the superconductor in vacuum, it can be shown that for samples of various shapes, the field at the surface of the sample will sometimes *exceed* the applied field $\mathbf{H}_a$, implying that some region of the sample will become normal before other regions, when H_a is close to H_c. See figure 2.1 for an schematic illustration. The result is that for fields in a range

$$1-\eta < \frac{H_a}{H_c} < 1\ ,$$

there will be a coexistence of superconducting and normal regions with field penetration, the so-called *intermediate* state. For example, the demagnetization factor η is equal to $\frac{1}{3}$ for a sphere, to $\frac{1}{2}$ for a cylinder in a parallel field, to 1 for an infinite slab in a perpendicular field, while it is 0 for a slab in parallel field. In this intermediate state, there are normal and superconducting domains, which interface has a given surface energy γ, given by [8]

$$\gamma = \frac{H_c^2\delta}{8\pi}\ , \tag{2.4}$$

where $\delta \approx \xi - \lambda$, the approximate thickness of the interface.

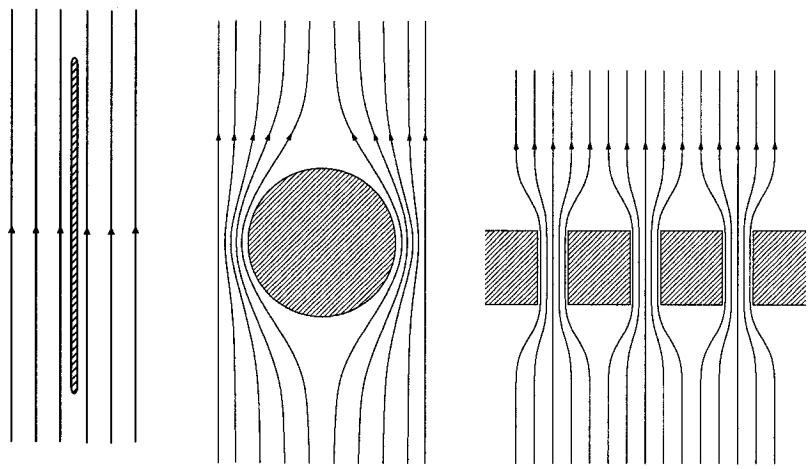

(a) (b) (c)

Figure 2.1: External field patterns when (a) η is almost 0 and when (b) it is $\frac{1}{3}$ for a sphere. The curvature in the field lines indicate that the field at the surface is larger than the applied field. In (c) $\eta = 1$ and clear distinct superconducting and normal domains are present. Adapted from [8].

2.3.4 Type II superconductors

The Ginzburg-Landau (G-L) theory (covered for example in Tinkham [8]), introduced a new parameter $\kappa = \lambda(T)/\xi(T) = a\lambda_L(0)/\xi_0$, the ratio of the penetration depth to the coherence length (a is a constant, equal to 0.96 (0.715) for pure (dirty) superconductors [8]). Abrikosov in 1957 [16] proposed a new classification of superconductors: superconductors of type I when $\kappa < 1/\sqrt{2}$ and of type II when $\kappa > 1/\sqrt{2}$. In the latter case, G-L theory leads to the result that the surface energy γ from equation (2.4) is *negative*. Abrikosov[2] showed that this negative surface energy causes the normal regions (which carry some flux) to subdivide until the flux carried by each region is equal to the flux quanta $\Phi_0 = hc/2e$. Those flux tubes, or vortices, are

[2] Aleixei A. Abrikosov, Vitaly L. Ginzburg and Anthony J. Leggett were awarded the 2004 Nobel prize in physics for "pioneering contributions to the theory of superconductivity and superfluids"

of size ξ, and are surrounded by a supercurrent screening the external field running over a length λ. Because of the repulsion between those opposite supercurrents, the vortices then arrange in a regular triangular array, the Abrikosov lattice. The flux penetration is continuous, from the first critical field H_{c1} the upper critical field H_{c2} where the transition to the normal state occurs. Unlike the intermediate state of type I superconductors as discussed in section 2.3.3, this so-called "mixed state" of type II superconductors occurs over a substantial field range (H_{c2} is much greater than H_c), even when the demagnetization factor $\eta = 0$. Abrikosov's discovery brought to light a remarkable new state of superconductors, bringing a new type of particles, the vortices. We will study until the end of this chapter the physics of vortices.

2.3.5 Basic vortex dynamics

Flux flow and pinning

In the mixed state, the superconductor is of course no longer a perfect diamagnet, but also loses its perfect conductivity. Since each vortex carries a flux quanta Φ_0 (it is interesting to note that the flux quanta Φ_0 is half the value of the fundamental quantum of flux of one electron: it is the flux quanta for a particle of charge $2e$, the Cooper pair), when a current density $\mathbf{J}$ is applied in the superconductor in the mixed state, the vortices will move under the action of the Lorentz force:

$$\mathbf{f} = \mathbf{J} \times \frac{\mathbf{\Phi}_0}{c} .$$

This will cause the flux lines to move tranverse to the current with a velocity $\mathbf{v}$, which in turn will lead to an electric field $\mathbf{E}$,

$$\mathbf{E} = \mathbf{\Phi}_0 \times \frac{\mathbf{v}}{c} ,$$

which is parallel to $\mathbf{J}$. See figure 2.2 for an illustration. Therefore there is a potential difference across the sample, implying the loss of perfect conductivity. In this "flux flow" regime, only a viscous drag limits the velocity of the vortices, and the resistivity follows the simple linear Bardeen-Stephen relation, $\rho = (B/B_{c2})\rho_n$, where ρ and ρ_n

are respectively the resistance in the mixed and normal state, and B is the applied field [8].

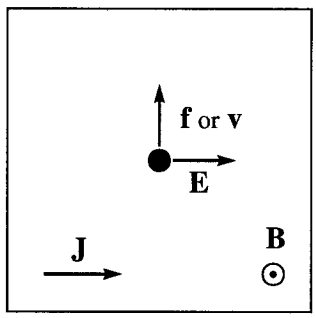

Figure 2.2: Schematic illustration of the forces acting on a vortex (represented by the black dot) when a current is applied in a superconductor

However, vortices are also under the action of pinning forces in the sample. Inhomogeneities or impurities of typical size ξ or λ in the superconductor will act as pinning centers for the vortices. Such spacial defects cause a local variation in ξ, λ or H_{c2} and thus in the free energy of the flux line, thereby favoring equilibrium at particular locations of the vortex. Thus in imperfect samples, vortex movement is triggered only when the current is sufficient to overcome the pinning forces. For currents under this "depinning" current or critical current J_c, the sample remains superconducting.

Such heavily pinned type II superconductors are ideal to make high field superconducting magnets. One frequently used material is NbTi: by bringing fine NbTi filaments in a copper matrix, one creates a fine-grained microstructure which pins the vortices, and the material can stay superconducting at current densities sufficient to produce fields up to 10T. On the other hand, weakly pinned superconductors like our amorphous samples $Fe_xNi_{1-x}Zr_2$ in which the flux flow regime is attained at low current densities are ideal systems for the study of the mechanisms of vortex motion and phases.

All in all, vortices in type II superconductors form quite a unique system to the fundamental researcher. Vortex matter form a crystal, in which the lattice parameter

can be varied by simply changing the external field, and in which one can change the driving forces on the particles by simply varying the current. Furthermore, since the vortex lattice lies within a real atomic crystal of much finer lattice constant, one can easily study the effects of disorder and thermal fluctuations which will influence the pinning response of the vortex crystal. The resulting phase diagram of disorder versus pinning force is quite fascinating, and many anomalies and perplexing phenomena come with the study of vortex physics. One of them is the peak effect, which we will cover in the next section.

2.4 The peak effect

The peak effect is observed as an anomalous enhancement of the critical current J_c just below the transitions at H_{c2} or T_c, in the vortex state of some low-T_c type II superconductors. It was discovered some 40 years ago, and while its origins are still under debate and under ongoing research, it is now generally accepted that it is the result of an order-disorder transition of the vortex lattice. The peak effect is usually seen in measurements of J_c as a function of temperature or field, but equivalently it can be observed as a drop in resistance (due to a vortex pinning phase which corresponds to the peak in J_c) as a function of magnetic field (or temperature) as it is done in this thesis with the $Fe_xNi_{1-x}Zr_2$ alloys. In some cases, this can lead to a surprising reentrance of the superconducting phase as the resistance sometimes drops to zero!

2.4.1 The vortex lattice

Before discussing the different mechanism proposed to be at the origin of the peak effect, we will first introduce some properties of the vortex lattice (VL). Firstly, the VL is not confined to the rigid Abrikosov triangular lattice. It can rather move under the action of a force or distort in order to lower its energy, *i.e.* the VL is elastic. This elasticity is essential to explain any pinning of the VL: if the VL were a perfectly rigid and periodic object, the random arrangement of pinning sites could never cause

any effective global pinning because as many pinning sites would exert a force in the direction of the Lorentz force as opposite to it. Therefore it is normal to consider the VL as an elastic object, subject to compressional, shear and tilt deformations.

The phase diagram for driven lattices in the presence of disorder is essential to understand the VL and is predicted in reference [17], and shown schematically in figure 2.3 for disorder as a function of driving force. At low driving force and disorder, one finds the Bragg glass phase. The latter has quasi-long range order and no topological defects. It is as good as a perfect lattice as far as translational order is concerned [4] and shows Bragg peaks in neutron diffraction experiments [18].

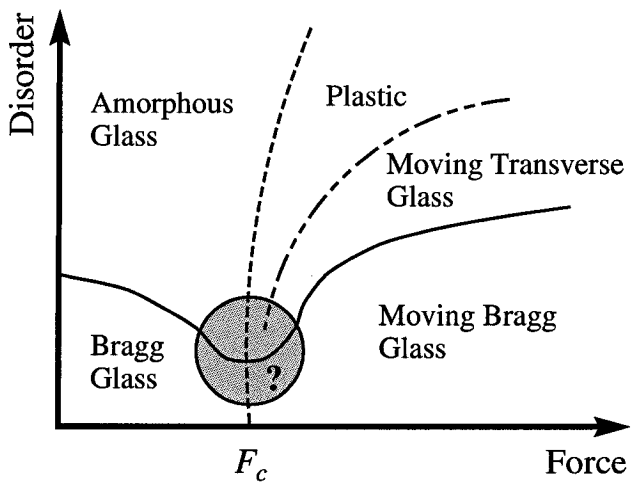

Figure 2.3: Schematic representation of the phases of the vortex lattice for different amounts of disorder, as a function of force on the vortices. Adapted from [17].

Upon application of a force greater than some critical force F_c, the Bragg glass becomes the moving Bragg glass (MBG), characterized by static channels in which the vortices flow. These channels are determined by the static disorder and do not fluctuate in time; they are the easiest paths the particle can follow without undue dissipation and are thus the result of a subtle competition between elastic energy, disorder and dissipation [4]. The vortices remain elastically coupled between different channels, and although the channels are rough, the MBG retains topological order.

Still for $F > F_c$ but for larger disorder strength, one finds the moving transverse

Glass (MTG). The MTG is still characterized by channels, however the vortices in different channels are now decoupled because of defects, and move almost independently. Dislocation are present beyond a certain length scale such that the lattice has a smectic topological order. Upon increasing the disorder further, one finds a phase characterized by a plastic flow of vortices. This phase contains pinned domains, which act as barriers which favors motion transverse to the direction of flow, such that the formation of long straight channels are prevented. Finally, going back to $F < F_c$, but now with larger disorder strength, one finds the amorphous glass phase. Its nature remains unclear, although it must contain topological defects and dislocations.

2.4.2 Proposed origins of the peak effect

Pippard and LO propositions

Sadly, most experimental studies conducted on the peak effect relied on transport measurements which, although they yield important information about the mobility of vortices and about the dynamics of pinning, are ill-suited for the study of thermodynamic phases transitions. Therefore, the interpretation of experimental data remains quite controversial and phenomenological.

A first qualitative explanation of the peak effect, which is the most accepted today, was proposed by Pippard [19] in 1969. He suggested that close to H_{c2} (or T_c), the VL would become softer, allowing the VL to become more distorted due to pinning forces. This would enforce strongly pinned vortices near H_{c2}, *i.e.* the vortices would sustain a larger force before motion is induced, and thus the critical current would be higher. Ten years later, Larkin and Ovchinnikov (LO) [20] proposed a more formal description of this explanation. It was said that the random disorder of the pins competes with and destroys the long range order of the VL, resulting in a short-ranged ordered VL. This loss of order has been observed in neutron diffraction experiments as the loss of Bragg peak intensity upon increase of the temperature through the peak effect [18, 21]. The LO theory introduced the correlation volume $V_c = R_c^2 L_c$, the volume of a VL domain within which the VL remains undistorted while between different

domains, shear and tilt distortions are favored by pinning. This volume depends on both the elasticity of the VL as well as the pinning:

$$\begin{aligned} R_c &= \frac{c_{aa}^{1/3} c_{66}^{2/3} r_f}{n_p \langle f_p^2 \rangle} \\ L_c &= R_c \sqrt{c_{44}/c_{66}} \end{aligned} \tag{2.5}$$

where c_{44} and c_{66} are respectively the tilt and shear elastic constants[3] of the VL, and r_f, n_p and f_p are respectively the range, density and elementary force of the pins. The pinning force is proportional to the critical current and given by

$$F_p = J_c H = \left(\frac{n_p \langle f_p^2 \rangle}{V_c} \right)^{1/2} = \frac{n_p^2 f_p^4}{r_f^3 c_{44} c_{66}^2} ,$$

using equation 2.5. In the LO model, F_p is almost field independent, because of a near cancelation of the factors $f_p \sim \Delta^2 \sim (H_{c2} - H)$ and $c_{66} \sim (H_{c2} - H)^2$, where Δ is the superconducting gap. LO further states that near H_{c2}, as the lattice parameter a of the VL decreases, and becomes much smaller than the range λ of inter vortex interaction so does R_c and V_c, and this yields nonlocal elasticity effects which induces a further softening of the lattice and decrease in c_{44}, and thus a rapid increase in F_p or J_c. At the peak, $R_c \sim a_p$ (the lattice constant at the peak), V_c becomes constant and the shutdown in F_p (the depinning) is due to the linear field dependence of f_p.

VL melting

For the sake of completeness we shall briefly present here another explanation of the peak effect present in the literature. In high-T_c cuprate superconductors, another type of peak effect has been observed. Its signature is very different than in the low-T_c systems: the peak effect is then seen as a sudden *increase* in the resistance versus field or temperature near H_{c2} or T_c. See for example reference [23]. In these systems, temperature fluctuations are much more considerable, and therefore the effect has been explained by a melting of the lattice into a disordered liquid phase, where

[3] one can describe the Hamiltonian of the VL as $H = \frac{1}{2\Omega} \sum_{\alpha\beta} \sum_q c_{\alpha\beta} u_\alpha(q) u_\beta(-q)$, where u is the displacement of a vortex from equilibrium, and $c_{\alpha\beta}$ the elastic constants. α, β are the spacial coordinates, q is the wave vector while Ω is a dimensional parameter. From [22].

thermal wandering of the vortices between pinning sites prevents pinning effects. A detailed description of the lattice melting is still lacking, but the classical Lindemann criterion as been applied to the cases of vortices in those superconductors. The VL melting happens when $< u^2 >= c_L^2 a^2$, that is when the mean square displacement u of the vortex from equilibrium is a considerable fraction of the lattice spacing a. c_L is the Lindemann parameter, which has found to be 0.1~0.2 for the high-T_c systems [24]. Similar values for low-T_c superconductors have been found (see for example reference [25]), however the value has been found to decrease for more dirty samples, an indication that disorder is not negligible. Whether the peak effect in low-T_c systems is due to a melting is disputable. As said earlier its signature is radically different: in the case of melting the peak effect leads to a decrease of pinning (a thermally induced melting transition) and thus to an increase in resistance, while in the LO case the pinning (a disorder induced melting transition) is increased and leads to a decrease in the observed resistance. Is it nevertheless possible that the peak effect in low temperature superconductors is due to the decrease in the LO correlation volume and a disordering of the VL triggered by both thermal fluctuation and disorder.

2.4.3 Associated phenomena

Bulk versus edge currents

In a rectangular shaped sample, the transverse flow of vortices tends to bring them at the edge of the sample. At these locations a greater force, or current, is necessary to give the vortices sufficient energy to cross the surface barrier, in order to enter or leave the sample and thus there should be an enhancement of the critical current at the sample edge. Furthermore, the surface barrier is in general non uniform, so that the distribution of vortices along the edges will also be non homogeneous, creating local nucleation and distortion in the VL. The current would create a disordered metastable phase at the edges, constantly annealed by the more ordered bulk phase. This phenomenom was called the "edge contamination mechanism" [26, 27], and must

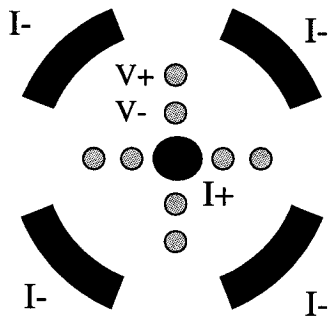

Figure 2.4: The Corbino disk contact geometry. The current flows radially and therefore the vortex movement is along a circle, creating a radial voltage. The symmetric configuration of the current contacts allows an isotropic current flow necessary to prevent the vortices to drift across edges of the sample

be linked with the peak effect.

It is possible to eliminate edge vortex contamination by using the Corbino disk contact geometry (see figure 2.4). In this geometry, vortices flow in circles and never come across the edges. Measurements done in reference [27] have shown a much sharper peak in critical current, a probable trace of a much sharper transition between the ordered and disordered LO phases.

Frequency of the driving current

The disordered phase at the onset of the peak effect (as J_c increases or as the resistance drops) is metastable. As discussed above, this phase is characterized by the edge contamination mechanism and is a dynamic coexistence of the disordered edge phase with the ordered bulk phase. By using higher frequency AC signal to look at the peak effect, it is possible to limit this contamination: the consequent vortex movement is of smaller amplitude. Conversely, low frequency or DC driving currents bring vortices into higher amplitude movements, allowing more edge effects and bulk contamination. The result of using high frequency signals is a sharper peak effect, similar to using the Corbino contact geometry, although not as drastic.

Chapter 3

Thermal Conductivity

3.1 Definition and general concepts

In an isotropic solid, heat flow obeys the relation

$$\mathbf{h} = -\kappa \vec{\nabla} T \ , \tag{3.1}$$

where $\mathbf{h}$ is the heat flow rate per unit area, T the temperature, and κ the thermal conductivity, in $\mathrm{Wm^{-1}K^{-1}}$. The negative sign indicates that the heat flows from hot to cold regions.

Equation (3.1) is a typical transport equation, which form is valid for electrical conductivity[1], diffusion, damping of sound, etc ... However in anisotropic materials, where heat flow is not necessarily parallel to the temperature gradient, the equation becomes tensorial:

$$h_i = \kappa_{ij} \frac{\partial T}{\partial x_j} \ ,$$

where the coefficients κ_{ij} now form a matrix.

In most cases and in this thesis, the method used to measure thermal conductivity is the steady state longitudinal flow, four probe measurement, illustrated schematically in figure 3.1. In this method, heat is supplied at one end of a sample, and flows longitudinally in a sample of constant cross section A, at a rate H, to the other

[1] Ohm's law $\mathbf{J} = \sigma \mathbf{E} = -\sigma \vec{\nabla} V$ is a similar transport equation.

end where is it entirely removed. Thermometers are attached at two locations on the sample, separated by a distance L to measure the temperature difference ΔT. Replacing H by power P per unit area, we obtain

$$\kappa = \frac{P}{\Delta T}\frac{L}{A} . \tag{3.2}$$

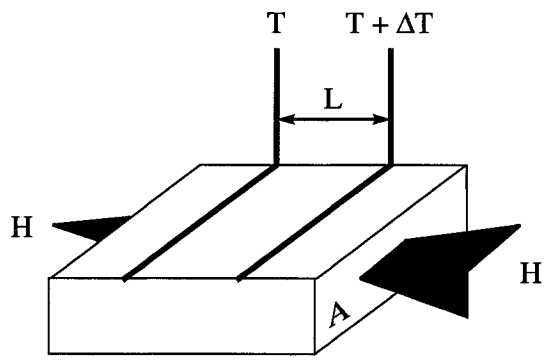

Figure 3.1: The longitudinal flow steady-state method used to measure thermal conductivity

Generally heat is conducted by conduction electrons and by lattice vibrations, but also by any energy excitations, or carriers, would they be vortices, spins, etc ... The thermal conductivity is then expressed as the sum of these various contributions:

$$\kappa = \kappa_{electrons} + \kappa_{phonons} + \cdots$$

These heat carriers move from the hot region to the cold region in the sample, and are scattered by other carriers, impurities or defects in the material. Considering those carriers as a gas diffusing through the material, and using the kinetic gas theory, we obtain the simple and intuitive relation

$$\kappa = \frac{1}{3} C_v v l , \tag{3.3}$$

where C_v is the specific heat per unit volume, v the velocity of the carriers and l their mean free path.

3.2 Phonons and the Boltzmann equation

Phonon thermal conduction is present in all solids, and is the preponderant conduction mechanism in non-metals and in amorphous systems. A good review of phonon thermal conductivity is given in Berman [28], from which most of this section is taken. Atoms in solids vibrate at certain modes or wave number q of given frequencies ω, and obey a dispersion relation $\omega(q)$, which will vary with atomic mass and crystal structure. The energy is propagated at the group velocity $v_G = dw/dt$. In quantum mechanics, a mode of frequency ω carries energy $(n + \frac{1}{2})\hbar\omega$, where n is any positive integer and $2\pi\hbar$ Planck's constant. Zero-point energy is $\frac{1}{2}\hbar\omega$ and the average of n, $\mathcal{N}^0$, also the number of thermally excited quanta of energy $\hbar\omega$, the phonons, is

$$\mathcal{N}^0 = \frac{1}{\exp(\hbar\omega/k_B T) - 1} , \tag{3.4}$$

according to Bose-Einstein statistics.

The heat current due to a mode q is given by the product of the thermal energy in that mode with the group velocity, and the total heat current is thus given by

$$\mathbf{h} = \sum \mathcal{N}(q)\hbar\omega \mathbf{v}_G(q) , \tag{3.5}$$

where $\mathcal{N}(q)$ is the number of phonons at mode q, the phonon distribution number. At thermal equilibrium $\mathbf{h}$=0 because both $\mathcal{N}^0$ and $\omega(q)$ are symmetric in q, and consequently $\mathbf{v}_G(-q) = -\mathbf{v}_G(q)$. Now with a temperature gradient, this is no longer the case. Suppose phonons travel in the z direction parallel to the gradient, and that at time t the number of phonons in some region is $\mathcal{N}(q)$. After δt these phonons have moved to the region $v_G^z \delta t$ away, and their number is now

$$\mathcal{N}(q) - v_G^z \delta t \frac{\partial \mathcal{N}}{\partial z} ,$$

so that the rate of change of phonon number is

$$\left(\frac{\partial \mathcal{N}}{\partial t}\right)_{drift} = -v_G^z \frac{\partial \mathcal{N}}{\partial z} = -v_G^z \frac{\partial \mathcal{N}}{\partial T}\frac{\partial T}{\partial z} \rightarrow -(\mathbf{v}_G \cdot \vec{\nabla} T)\frac{\partial \mathcal{N}}{\partial T} , \tag{3.6}$$

in three dimensions.

In a steady state at a constant temperature gradient, the phonon density in the solid must become independent of time. There must therefore be other processes which oppose this constant drift. We can identify these as scattering processes, so that we obtain the Boltzmann equation

$$\left(\frac{\partial \mathcal{N}}{\partial t}\right)_{drift} + \left(\frac{\partial \mathcal{N}}{\partial t}\right)_{scatt.} = 0 \,. \tag{3.7}$$

Such an equation is quite difficult to solve for $\mathcal{N}(q)$. One often makes the relaxation time approximation. It is simply assumed that a scattering process will restore the phonon distribution towards its equilibrium value exponentially, with a relaxation time τ_q which depends on q:

$$\left(\frac{\partial \mathcal{N}}{\partial t}\right)_{scatt.} = \frac{\mathcal{N}^0 - \mathcal{N}}{\tau_q} \,. \tag{3.8}$$

By assuming that the distribution $\mathcal{N}$ is left almost unchanged from its equilibrium value in the presence of a temperature gradient, we can replace it by $\mathcal{N}^0$ in the drift term (equation 3.6). Using this in the Boltzmann equation (3.7) and combining it with equation (3.8), we obtain

$$v_G^z \frac{\partial \mathcal{N}^0}{\partial T}\frac{\partial T}{\partial z} = \frac{\mathcal{N}^0 - \mathcal{N}}{\tau_q} \,. \tag{3.9}$$

This equation is easily solved for $\mathcal{N}$, and combining equation (3.9) with the heat current (equation 3.5), yields (the sum term with $\mathcal{N}^0$ vanishes)

$$h = -\sum \hbar\omega (v_G^z)^2 \tau_q \frac{\partial \mathcal{N}^0}{\partial T}\frac{\partial T}{\partial z} \,,$$

which in turn gives the phonon thermal conductivity

$$\kappa_{ph} = -\frac{h}{\partial T/\partial z} = \sum \hbar\omega (v_G^z)^2 \tau_q \frac{\partial \mathcal{N}^0}{\partial T} \,.$$

We can replace the summation by an integral over ω and write $(v_G^z)^2 = \frac{1}{3}v_G^2$ for an isotropic material, to obtain

$$\kappa_{ph} = \frac{1}{3}\int_0^{\omega_{max}} \hbar\omega v_G^2 \tau_q \frac{\partial \mathcal{N}^0}{\partial T} \mathrm{f}(\omega)\mathrm{d}\omega \,, \tag{3.10}$$

where $\mathrm{f}(\omega)\mathrm{d}\omega$ is the phonon density of states, and ω_{max} the maximum phonon frequency in the dispersion relation spectrum.

The computation of the thermal conductivity from equation (3.10) is still quite difficult, as it necessitates the knowledge of the dispersion relation $\omega(q)$. The latter is very complicated to obtain. In general there are three dispersion curves corresponding to the three possible polarization directions (two longitudinal and one transverse), and the total number of different modes is $3N$ if there are N atoms in the crystal (one for each degree of vibrational freedom). Furthermore, if not all the atoms are the same, or if the lattice structure has more than one atom per unit cell, the modes will be split among different frequency bands: the optic band of high frequencies and the acoustic band ranging from zero upwards.

Consequently, it is very convenient to use the simple Debye model, which gives good results according to experiment. The Debye theory assumes a simple linear dispersion relation $\omega(q) = vq$ for the phonon spectrum, which is valid for small q in crystals, and also that the phonon velocities are the same for the three polarization. Having [28]

$$\mathrm{f}(\omega)\mathrm{d}\omega = \frac{3q^2}{2\pi^2}\mathrm{d}q \ ,$$

we obtain

$$\mathrm{f}(\omega)\mathrm{d}\omega = \frac{3\omega^2}{2\pi^2 v^3}\mathrm{d}\omega \ . \tag{3.11}$$

From equation (3.4), we have

$$\frac{\partial \mathcal{N}^0}{\partial T} = \frac{(\hbar\omega/k_B T^2)\exp(\hbar\omega/k_B T)}{[\exp(\hbar\omega/k_B T)-1]^2} \ ,$$

so that using equations (3.10) and (3.11), with $x = \hbar\omega/k_B T$, we obtain

$$\kappa_{ph} = \frac{k_B}{2\pi^2 v}\left(\frac{k_B}{\hbar}\right)^3 T^3 \int_0^{\theta/T} \tau(x)\frac{x^4 e^x}{(e^x-1)^2}\mathrm{d}x \ , \tag{3.12}$$

where $\theta = \hbar\omega_{max}/k_B$ is the Debye temperature. Some insight might be added by considering the contribution to the heat capacity from modes in the range ω to $\omega + \mathrm{d}\omega$ as the derivative $(\mathrm{d}/\mathrm{d}T)[\hbar\omega\mathcal{N}^0\mathrm{f}(\omega)\mathrm{d}\omega]$ so that in terms of x and in the Debye approximation,

$$C(x)\mathrm{d}x = \frac{3k_B}{2\pi^2 v^3}\left(\frac{k_B}{\hbar}\right)^3 T^3 \frac{x^4 e^x}{(e^x-1)^2}\mathrm{d}x \ .$$

Expressing the relaxation time as the ratio of the mean free path l to the velocity v, we obtain the logical extension of the kinetic equation (3.3),

$$\kappa_{ph} = \frac{1}{3} v \int l(x) C(x) \mathrm{d}x \ . \tag{3.13}$$

3.3 Electrons and the Wiedemann-Franz law

A very similar demonstration seen in the previous section can be used to derive the electronic thermal conductivity. It is found in Ashcroft and Mermin [29]. We will here only outline the results, which are very similar to the Drude theory of a free electron gas [28]. We have

$$\kappa_e = \frac{1}{3} c_e v_F^2 \tau \ , \tag{3.14}$$

where v_F and τ are respectively the Fermi velocity of electrons and the relaxation time. We have a linear T dependance for the heat capacity c_v:

$$c_e = \frac{\pi^2}{2} N k_B \frac{k_B T}{E_F} \ , \tag{3.15}$$

where N is the number of electrons and E_F the Fermi energy.

The expression for electrical conductivity can also be obtained in a similar manner [28], and is equal to the Drude result

$$\sigma = \frac{n_e e^2 \tau}{m_e} \ , \tag{3.16}$$

where m_e, e and n_e are respectively the electron mass, charge and density. In the free-electron model, we have the common expression for the spherical Fermi surface [29],

$$\frac{4\pi}{3} k_F^3 = 4\pi^3 n_e \ . \tag{3.17}$$

Using equations (3.14), (3.15), (3.16) and (3.17), and assuming τ is the same for heat and electrical conduction scattering processes, we obtain the Wiedemann-Franz (WF) law

$$\frac{\kappa}{\sigma T} = \frac{\pi}{3} \left(\frac{k_B}{e} \right)^2 \equiv L_0 \ , \tag{3.18}$$

where $L_0 = 2.44 \times 10^{-8} \mathrm{W} \cdot \Omega/\mathrm{K}^2$ is the Lorentz number. This assumption is however not always valid. When an electric field is turned on, there is a net drift of electrons in one direction, and we can use the Boltzmann equation 3.7 to find the relaxation time of the scattering processes. However when a thermal gradient is applied, the drift of electrons is a priori zero. On the hot side there will be more high energy electrons and few low energy electrons with respect to the cold side. The result is an electron drift from hot to cold and vice versa which cancel out, but will tend to change the net thermal equilibrium on each side. Therefore, there has to be corresponding scattering processes of sufficient intensity to prevent this. Berman [28] suggests that electron-phonon scattering processes will not be able to provide the necessary changes in electron energy, and therefore at low temperatures, and in systems such as amorphous systems were the dominant scattering of electrons comes from phonons, less heat will be transported to the cold side. This implies that the WF law will overestimate the electronic thermal conductivity. However at higher temperatures or in dirty samples where defect scattering dominates, electron-phonon scattering is less important, the WF law will hold.

3.4 Scattering processes

As a transport property, thermal conductivity is highly dependant on the various scattering mechanisms. The effects of scattering are to change the temperature dependance of κ, and we will give here an overview of these effects. Of particular interest are the phonon scattering mechanisms, present in amorphous systems. A good review of scattering in solids is found in Berman [28] and in the thesis of Legault [30].

3.4.1 Scattering of electrons

Impurities and defects

Electron-impurity scattering is considered elastic since the change in energy of the impurity is much smaller than the initial energy of the electron. Consequently, the

relaxation time is mostly temperature independent, and therefore κ_e remains linear in T.

Electron-phonon scattering

Electron-phonon scattering is very difficult to evaluate, and it has been found [28] that the scattering rate is given by

$$\frac{1}{\tau_{ep}} = constant \times \omega \ ,$$

which upon insertion in equation 3.12 and following integration, yields

$$\kappa_{ep} \propto T^2 \ ,$$

which is the same temperature dependance due to two level systems present is amorphous solids, as will be shown in section 4.2.2.

Electron-electron scattering

Electron-electron scattering is usually negligible and only present in very pure and perfect crystals. From the start, the Rutherford cross section is very small ($\sim 10^{-9}\mathrm{m}^2$ for ordinary metals) [28], and it is further decreased by the Pauli exclusion principle: in order that spin, charge, energy are conserved in a collision between two initial and final electron states severely restricts the possible states combinations. The cross section is then further reduced by a factor $\sim (k_B T/E_F)^2 \approx 10^{-4}$ at room temperature [28, 31]. The T^2 term in the scattering cross section brings a T^2 contribution to the resistivity ρ_e and thus a linear temperature in κ_e when using the WF law [28].

3.4.2 Scattering of phonons

Boundary scattering

At low temperatures, the mean free path of the phonons is very long, because the solid, near to its ground state has only low-energy phonons, which therefore have long wavelengths. This wavelength is then much larger than the solid's order (structure +

defects) and even of the sample size, and phonons act as sound waves traveling through air with very few scattering events. The scattering rate can then be approximated as

$$\frac{1}{\tau_{boundary}} = \frac{v}{l_{max}} ,$$

where v is the average phonon velocity and l_{max} the maximum mean free path. Inserting this relaxation time into equation 3.12 and integrating, we obtain

$$\kappa_{boundary} \propto l_{max} T^3 .$$

It has been found that l_{max} depends as expected on the dimension of the sample, in the following way: $l_{max} \propto \sqrt{thickness \cdot width}$ [30, 32]. One needs also to consider the roughness of the sample since for very well polished sample there will be specular reflection of phonons which will increase l_{max} while conversely a rough sample will add dislocations which will induce scattering and shorten l_{max}. However the roughness factor is difficult to evaluate.

Point defects

Scattering of phonons on defects was first calculated by Klemens in 1955 [33] and found in [30]. We outline here the results. As seen in section 3.2, we have $\theta_D = \hbar\omega_{max}/k_B$, from which we can derive

$$\frac{\theta_D}{T} \approx \frac{\omega_{max}}{\omega} \approx \frac{\lambda}{\lambda_{min}} , \tag{3.19}$$

where the minimum possible wavelength λ_{min} of the phonons is the interatomic distance, a few nm. From this equation 3.19, we see that when $T \ll \theta_D$ (in which case $\lambda_{min} \ll \lambda$), only defects of atomic size can be considered as point defects to most phonons. Such defects are: a vacancy in a lattice site, a substitution atom, and interstitial atom ... or a combination of these. The resulting distortions in the lattice, or the differences in atomic mass or bonding causes additional scattering [28]. Klemens found that the scattering rate was proportional to ω^4, an analogous result obtained in 1896 by Raleigh (and known as Raleigh scattering) when he calculated the scattering

of sound waves by an obstruction of dimensions small compared with the wavelength. Using equation 3.12, point defects give a contribution to the thermal conductivity

$$\kappa_{pd} \propto T^{-1} .$$

Phonon-phonon scattering

If the atomic potential energy in perfect solids were to be perfectly harmonic, phonons would have an infinite lifetime and would propagate without interacting with one another. In the absence of any other scattering, the conductivity would then be essentially infinite. However even in the purest and defect-free crystals one expects to see a finite conductivity, and therefore phonons will interact, because of anharmonic (cubic, quartic or higher powers of the displacement) lattice forces. Phonon-phonon interaction involves the annihilation of two phonons of respective wave number and frequency ($\mathbf{q}_1$, ω_1) and ($\mathbf{q}_2$, ω_2) to create a phonon ($\mathbf{q}_3$, ω_3), such that

$$\omega_1 + \omega_2 = \omega_3 \qquad \text{and} \tag{3.20}$$

$$\mathbf{q}_1 + \mathbf{q}_2 = \mathbf{q}_3 + \mathbf{g} , \tag{3.21}$$

where $\mathbf{g}$ is a reciprocal lattice vector or 0. The derivation of these equations was done by Peierls [34], and found in [30]. Cubic terms in the potential involves 3 phonons modes like in the above case, while quartic terms will involve 4 phonon modes, and etc.... Processes with $\mathbf{g}$=0 are called normal or N processes while those for which $\mathbf{g} \neq 0$ are called U (Umklapp - "turn down" in German-) processes. We shall look the effects of these processes on the thermal conductivity.

Normal processes

N-processes preserve energy and crystal momentum (equations 3.20 and 3.21) and cannot create thermal resistance, because although the phonon distribution changes, the net phonon momentum in a certain direction is unchanged. However, N processes do have a subtle effect on the thermal conductivity: it changes the frequency distribution of the phonons, when for example two low frequency phonons are replaced by

a high frequency one or vice-versa. Since the scattering rates of other processes are in general frequency dependent (as seen in this and the previous sections), those will be changed, influencing the thermal conductivity.

So N processes do not tend to restore the equilibrium distribution function, and the relaxation approximation 3.8 is not applicable. Therefore one cannot use equation 3.12 with some τ to calculate the effects of N processes on κ. The most widely used treatment in that subject is the one of Callaway developed in 1959 [35] and found in [28]. He assumed that N processes restore an arbitrary phonon distribution, with relaxation time τ_N. He assigned a time τ_R for all the remaining scattering processes, so that we can write the total scattering rate $\tau^{-1} = \tau_R^{-1} + \tau_N^{-1}$ using Matthiessen's rule.

The temperature dependence of the τ_N has not been established clearly. Herring [36] suggests that at low temperatures, $\tau_N^{-1} \propto \omega^n T^{5-n}$, where n is an integer between 1 and 4 which depends on the phonon polarization and lattice structure. In any case this factor is quite difficult to calculate and to measure.

Umklapp processes

U processes occur when the total momentum of a phonon-phonon collision is shifted by a lattice vector $\mathbf{g}$. Its effects are noticeable in perfect and imperfect crystals as the thermal energy can then be transported in a quite different direction. It has been found that at high temperatures, $\kappa \propto 1/T$, while at very low temperatures far from θ_D, only small fraction of phonons (with energy $\sim 4k_BT$) take part in U processes, so that $\kappa \propto T^{\epsilon} e^{\theta_D/bT}$, where ϵ and b are of the order of unity [28].

These results hold for crystals with a well-defined unit cell. Of more interest for our amorphous materials is the result of Kalugin *et. al.* [37] and found in [30] which takes into account U processes in quasicrystals. He has found that the scattering rate due to U process is more power law like than exponential at low temperatures:

$$\frac{1}{\tau_{Uqc}} \propto \omega^2 T^4 ,$$

yielding a temperature dependence to the thermal conductivity $\sim T^5$. Quasicrystals

have a longer range order than amorphous systems, evident from sharp diffraction peaks, but have little translational symmetry because they have a 5-fold pentagonal crystalline symmetry, a forbidden 3-D symmetry group. Although they have a structure similar to a crystal, their electronic and phononic properties are similar to those found in amorphous systems.

Other mechanisms

They are other mechanisms responsible for phonon scattering. Among them are dislocation, stacking faults, large defects etc... They don't play a priori an important role in amorphous materials.

3.5 Thermal conductivity in superconductors

3.5.1 Electronic thermal conductivity

As we have seen in section 2.2, electrons in the superconducting state form Cooper pairs. The Cooper pairs cannot scatter any impurities, phonons or normal electrons and carry no entropy. Therefore, below T_c, we expect to see the electronic thermal conductivity to decrease drastically as the number of cooper pairs increases, or as the number of normal electrons (also called quasiparticle excitations form Fermi-liquid theory) decreases.

In the BCS theory, it is found that the specific heat follows an exponential decrease in temperature with a characteristic decay $\sim \Delta_0/k_B$. This happens when $T <\sim 0.4T_c$ [28], basically because the decrease in normal electron number is also exponential. Therefore on the simple assumption of the kinetic equation 3.14, the behavior of the electronic thermal conductivity should be exponential as well at low temperatures. Furthermore, since the superconducting transition is a second-order phase transition, there is a jump is the heat capacity at T_c (of relative value 1.43 in BCS theory [7]), which should be reflected in the electronic thermal conductivity by a discontinuity at T_c. Although this discontinuity is hardly seen, a detailed analysis carried out by

Geilikman in 1958 [38] and seen in [7] on the basis of the BCS theory leads to the following result:

$$\frac{\kappa_s}{\kappa_n} = \frac{6}{\pi^2}\left[\frac{\Delta_0^2/T}{e^{\Delta_0/T}+1} + 2T\sum_{s=1}^{\infty}\frac{(-1)^{s+1}}{s^2}e^{-s\Delta_0/T} + 2\Delta_0\ln(e^{-\Delta_0/T}+1)\right],$$

where κ_s and κ_n are the electronic thermal conductivity in the superconducting and normal state, respectively, Δ_0 the superconducting gap at T=0, and k_B is set to unity. This theory is in good agreement with experiment [7].

3.5.2 Lattice thermal conductivity

The superconducting transition does not change the state of the lattice and the number of phonons depends on the temperature as in the normal solid. However the lattice thermal conductivity will be changed if electron-phonon scattering was important in the normal state. This is usually the case at low temperatures, in disordered superconductors where phonon thermal conductivity is dominant. What is seen in this scenario is an increase in the thermal conductivity below T_c. The exponential decay of the number of quasiparticle excitations results in the corresponding growth in the phonon mean free path $l \rightarrow l_{e-ph}$ and thus in the phonon thermal conductivity . As expected this growth is not endless: as soon as l_{e-ph} becomes larger than the mean free path related to other processes such as boundary or impurity scattering, those processes become dominant and the thermal conductivity decreases.

3.5.3 Vortex thermal conductivity

As seen in section 2.3.4, vortices in superconductors correspond to tubes of size ξ in the normal state which carry the flux quanta $\Phi_0 = hc/2e$, surrounded by a supercurrent running over the length λ. Within the core of the vortex, the energy gap $\Delta(r)$ is suppressed, and the quasiparticles (renormalized normal electrons) can be thought of obeying Schrödinger equation in a potential $\Delta(r)$. In s-wave superconductors (when the gap is isotropic, like in BCS superconductors), the corresponding eigenstates form bound states around the vortex core, with spacing Δ^2/E_F [39, 40]. As the field is

increased, the vortex density increases, enhancing the bound state overlap, resulting in the formation of energy bands that allow the intervortex transfer of quasiparticles [41, 42, 43, 44]. This is expected to influence experiments on thermal transport or heat capacity, which are sensitive to quasiparticle excitations.

At low fields, the vortices are well separated and the bound states are localized around the vortex core, so that the electronic thermal conductivity is not expected to vary much from its zero-field value. On the other hand, in increasing field, the quasiparticle bound states start to be more and more delocalized, thus capable of conducting heat, and we should expect an increase in κ_e. That holds whenever the gap is isotropic: in anisotropic gaps (d-wave superconductors such as the high-T_c materials) where the gap is smaller in certain directions, the delocalization can happen at much lower fields. Studying the field dependence of κ_e thus provides a mean to detect the gap structure. Scattering of electrons on vortices has also been considered [45], and sadly little information is available about the effect of vortices on the lattice thermal conductivity .

Chapter 4

Amorphous Solids

4.1 Introduction

The fundamental differences between the crystalline and amorphous solids states lies in their microscopic atomic structure. In crystals the atomic positions are arranged in a translationally periodic lattice, which exhibit short and long range order, and possesses a well-defined unit cell. In contrast, an amorphous solid exhibits an *infinite* unit cell, the atomic structure having only short range order. This is illustrated in figure 4.1. As we can see in figure 4.1(b), the atomic array in an amorphous solid is highly disordered, but not random, at least on a short length scale of a few interatomic distances. Over such a length (typically ~2-5 nm), the amorphous system has a considerable degree of local correlation, even though it lacks global periodicity. Randomness is more properly associated with gasses as in figure 4.1(c), where the atomic positions in space are totally uncorrelated. The presence of chemical bonding between the atoms of a solid, resulting in highly directional covalent bonds, is usually responsible for this local order [46].

Amorphous solids have a structure very similar to liquids apparent from X-ray diffraction patterns. This similarity is evident from the preparation procedure of *glasses*. The term glass is conventionally reserved for an amorphous solid produced by quenching of the melt. In such a case, a liquid is cooled sufficiently rapidly past the melting temperature T_m, so that the time and energy required for nucleation and

growth of crystallites is inadequate and the crystallization is bypassed. Thus, the liquid phase persists until a lower temperature is reached. At this glass transition temperature T_g, the supercooled liquid is effectively a solid because the time needed for configurational relaxation becomes too long on a laboratory time-scale [47, 48, 49]. In other words, liquid-like structural disorder is frozen into the glassy solid. The supercooled liquid is a metastable phase: if sufficient energy such as heat is applied to it, so that its temperature lies between T_g and T_m, it will re-crystallize, first macrocospically as micro crystals form into the amorphous matrix [46].

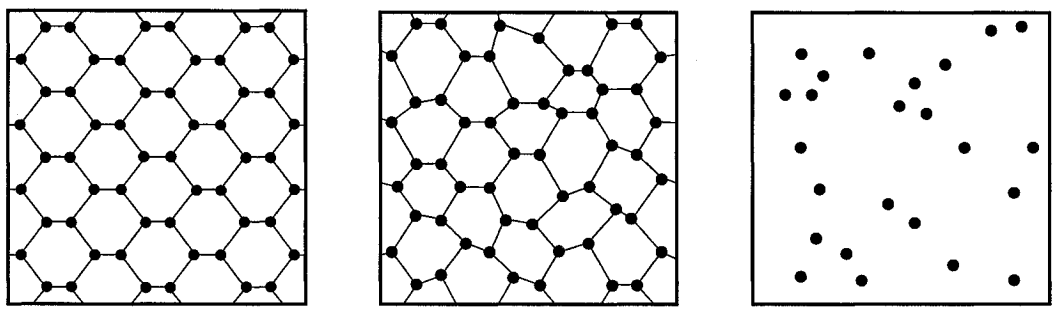

(a) (b) (c)

Figure 4.1: A schematic diagram of atomic arrangements in (a) a crystalline solid, (b) an amorphous solid and (c) a gas. Adapted from [47].

We won't go here in the details of the theory of metallic glass formation, but metallic glasses are more difficult to make than their insulating counterparts (like silicium-oxide alloys, the common household glass), necessitating cooling rates above 10^5 K/s like in the case of our Fe-Ni-Zr alloys. To date, no pure metal has been rapidly solidified to give a glass. Metallic glasses were first produced in 1960 by Duwez *et. al.* at Caltech [50, 51] and brought at the time totally novel exotic materials, ones that exhibited metallic-like properties (electrical, thermal and mechanical), albeit in a non-crystalline matrix. They also brought some possible interesting applications, as their mechanical and chemical properties proved to be better than traditional crystalline materials. Large scale applications of amorphous metals, which would have led to a replacement of the conventional FeSi transformer magnets, looked promising in the

1980s, but to date the conventional systems have won the economic competition. In fact, in addition to the difficulty of preparing bulk amorphous metals, one of their main shortcomings is the "aging" phenomenon. The ultra-soft magnetic properties of the amorphous shielding could only be kept for long periods of time if the system was treated very cautiously, both thermally, magnetically and mechanically, as the material properties of amorphous metals would otherwise deteriorate significantly after cycle times of several months or years [52].

Nevertheless, in the 1970s, Zeller and Pohl [53] showed unambiguously that below 1 K, the thermal properties of amorphous materials differed significantly from their crystalline counterparts, thereby triggering large interest in the scientific community. Among the many theories proposed at the time, this anomalous character of amorphous systems is now generally believed to be the cause of two level systems or tunneling states. We will look in the next section this theory, as well as the corresponding low-temperature thermal properties of amorphous solids.

4.2 Low temperature properties of amorphous solids

Before 1970, most solid-state physicists would have predicted that the low temperature heat capacity or thermal conductivity of some glass would have been similar than its crystalline counterpart, on the grounds that at low temperature, the structural irregularities in glasses become progressively less important as the phonon wavelength increases. Instead, it was shown by Zeller and Pohl that for oxide glasses, the heat capacity and thermal conductivity respectively varied linearly and as T^2, instead of the Debye and much faster T^3 prediction as expected from the phonon contribution to those quantities. Furthermore, the absolute values of the heat capacity and thermal conductivity laid within an order of magnitude *for all* amorphous solids, suggesting that there was an universal phenomenon responsible for the particular physics of amorphous systems. We will discuss in the next sections the theory behind those anomalies, on the specific heat and thermal conductivity. An extensive review of the low temperature properties of amorphous systems is given in the book edited by W.A.

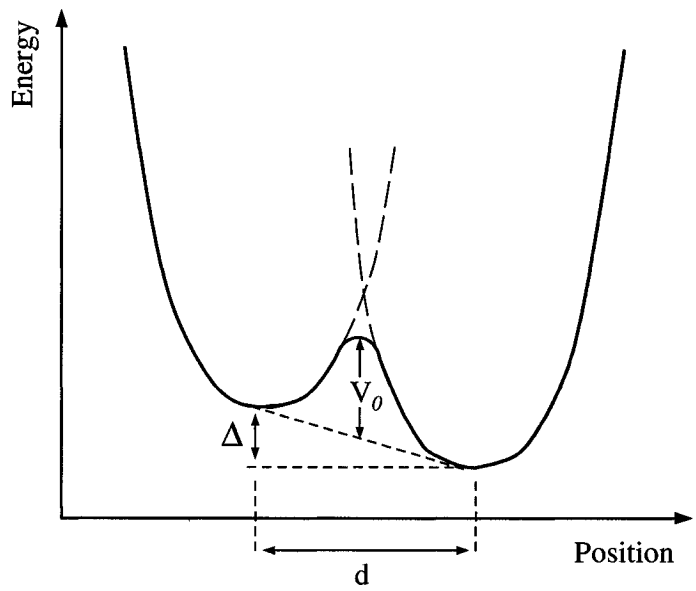

Figure 4.2: An asymmetric double-well potential built up from two harmonic oscillator potential (continued as dotted lines) for atoms in amorphous systems. The parameters Δ (the asymmetry energy), V_0 (the barrier height) and d (well minima separation) are also indicated. Adapted from [55].

Phillips [54].

4.2.1 Two level systems

More than ten models where suggested following this discovery. Of all the models only the tunneling state model proposed independently in 1972 by Anderson, Halperin and Valma [5] and by Phillips [6], a generalization of the two-level system (TLS), was able to explain the thermal and acoustic data. This model assumes that in a disordered solid, as opposed to a crystalline one, certain atoms or group of atoms have available two or more accessible potential minima. These atoms move in a potential of the form shown in figure 4.2. This scenario is a reflection of the fact that in amorphous solids, atoms have many possible equilibrium positions due to the short range order, as illustrated in figure 4.3. At low temperature, only the two lowest energy levels are significant, with an energy difference determined by the quantum mechanical

tunneling through the potential barrier V_0 and asymmetry Δ. In fact, the two lowest states have energy $\pm E/2$, where

$$E^2 = \Delta^2 + \Delta_0^2 ,$$

where the coupling energy Δ_0^2 is the energy difference between the lowest states in a symmetric double-well, and is related to well energy V_0 and separation of minima d by

$$\Delta_0 = \hbar\Omega e^{-\lambda} ,$$

where

$$\lambda = \sqrt{2mV_0/\hbar^2}d ,$$

where Ω is equal roughly to ω_0, the frequency of oscillation in a simple harmonic single well, and m the mass of the particles in the well. The exponential factor represents the overlap between the wavefunctions for the two wells [54, 55]. Now the free energy of a TLS may be written as [6] as

$$F(E) = -k_B T \ln\Big[\cosh(E/2k_B T)\Big] ,$$

and since the specific heat is given by $-T(\partial^2 F/\partial T^2)$, the total specific heat is given by an integration over all two level systems:

$$C = k_B \int_0^\infty n(E)\left(\frac{E}{2k_B T}\right)^2 \mathrm{sech}^2\left(\frac{E}{2k_B T}\right)\mathrm{d}E , \tag{4.1}$$

where $n(E)$ is the density of TLS per unit volume and energy interval. In the more general case of tunneling states, there is a distribution of values of Δ_0 (or λ or V_0) as well as E and therefore in this case we should add an integral over this parameter. However in practice this distribution is unknown and this further averaging is neglected. Phillips [6] suggests that in the range of energies of interest (between 0.1 and 1K, *i.e* for E between 10^{-5} and 10^{-4} eV), the density of states can be taken as a constant, n_0, so that equation 4.1 can be evaluated to give

$$C = \frac{\pi^2}{6}k_B^2 n_0 T .$$

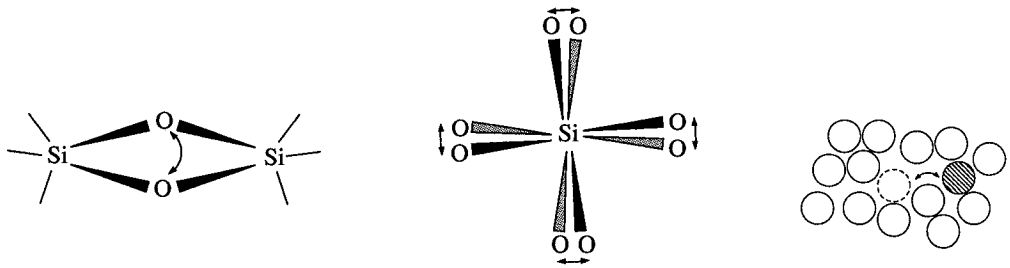

(a) (b) (c)

Figure 4.3: Microscopic model for two-level systems in glasses: (a) atom flip, (b) structural unit rotation and (c) atom-vacancy exchange in glassy metals. Adapted from [55].

So we see that the TLS model accounts naturally for the anomalous linear term in the specific heat when a constant density of tunneling states is assumed. This linear term can be confused with the electronic contribution to the heat capacity which has the same temperature dependence. However it was shown by Graebner *et. al.* [56] to persist in superconducting glasses, well below T_c where the electronic contribution to C is essentially zero.

4.2.2 Thermal conductivity

The TLS model is also capable of explaining the anomalous T^2 temperature dependence of the thermal conductivity observed in glasses at low temperatures. Phonons of energy $\hbar\omega = E$, the TLS splitting, can be scattered by a TLS by a process of excitation from the ground state and subsequent spontaneous decay and emission of an incoherent phonon, *i.e.* resonance scattering [55]. Assuming again a constant density of TLS, it can be shown [54] that the scattering rate of phonons scattered in such a manner is given by

$$\frac{1}{\tau_{TLS}} = \frac{\pi n_0 M^2 \omega}{\rho v^2} \tanh\left(\frac{\hbar\omega}{2k_B T}\right), \tag{4.2}$$

where v is the average phonon velocity, M the coupling constant between the phonon wave to the TLS and ρ the mass density of the solid. Substituting equation 4.2 in equation 3.12 (or in 3.13 together with the linear heat capacity: $l = v\tau$) yields a T^2

dependence on κ.

Resonance scattering by itself is not always sufficient to explain thermal conductivity data in amorphous solids, especially at higher temperatures where plateaus in κ have been observed. There is an additional scattering mechanism that is exhibited by TLS. Just like any two-level systems, like 1/2 spins in a magnetic field, the rate at which equilibration of the level take place after a change in population is given by T_1^{-1} [54], where

$$T_1^{-1} = \frac{M^2\omega^3}{2\pi\rho\hbar v^5} \coth\left(\frac{\hbar\omega}{2k_BT}\right),$$

which yields a non-resonant scattering rate $T_1^{-1} \propto T^3$ [54], and the net scattering rate is thus $\tau^{-1} = \tau_{TLS}^{-1} + T_1^{-1}$. Basically the non resonant term limits the increase in mean free path in temperature resulting from resonant scattering ($l_{res} \sim T^{-1}$), and can give rise to a plateau in the thermal conductivity.

It should be noted that many amorphous systems don't display a totally linear heat capacity nor a totally quadratic thermal conductivity. Experiments rather show that $C \propto T^{1+m}$ and that $\kappa \propto T^{2-m}$ [55]. This can be accommodated by relaxing the plausible but simplistic assumption that $n(E)$ is energy independent, and assuming instead that it is only weakly dependant on energy such that $n(E) \propto E^m$, where $m = 0.1 - 0.3$ [55]. Furthermore, it should be also noted that although the tunneling or TLS model is phenomenologically very successful, the microscopic origin of the TLS is still unknown. Some possible causes are schematically illustrated in figure 4.3.

Chapter 5

Experimental Details

This chapter will present the details of the experimental methods employed in this study. We will present a description of the $Fe_xNi_{1-x}Zr_2$ alloys preparation along with a report of their properties. We will follow with a description of the apparatus used for low-temperature measurements and for thermal conductivity measurements. A discussion on the source of errors which have to be considered in the analysis will conclude the chapter.

5.1 The $Fe_xNi_{1-x}Zr_2$ alloys

The amorphous Fe-Ni-Zr superconducting alloys used in this study are made from the rapid quenching of the melt as briefly described in section 4.1. It has only been approximately 20 years since the high cooling rates necessary to properly form glassy metals have been achieved and, as we have seen, those materials posses remarkable low-temperatures properties. Furthermore, prior to that time superconductivity was a business of mostly crystalline materials. But the long range order of crystalline materials favors strong collective pinning, such that crystals typically have a high critical current. This forces one to use large currents before any flow of vortices can take place, and the linear flux flow regime can difficultly be probed [4]. In general, strong pinning will limit the investigatitions of the pinning/depinning mechanisms of the vortex lattice, a facet of superconductivity which remains obscure. The Fe-Ni-Zr

metal superconducting glasses, being amorphous, have a much lower critical current, which permits a more interesting study of the vortex lattice dynamics [4]. They have a very weak pinning potential and critical current, with $J_c \leq 0.4$ A/cm^2 [3] about 100 to 1000 times smaller than the widely studied crystalline 2H-$NbSe_2$ [57] and others [19, 23, 58, 59, 60, 61], and 10 times smaller than other amorphous films samples [62, 63, 64, 65], confirming the high purity of the samples.

5.1.1 Some physical properties

Not much is known about the superconducting state of the $Fe_xNi_{1-x}Zr_2$ alloys. No studies have been made so far on the superconducting energy gap to determine whether it is of the BCS type or not. However it behaves like a standard superconductor and we can assume that it is a BCS type-II superconductor.

An amorphous superconductor can be considered as a crystalline superconductor with many impurities, in the so-called dirty limit. In the dirty limit, the ratio of the mean free path l to the coherence lenght ξ_0 of the material is small ($\ll 1$), wheras in the clean limit it is large ($\gg 1$). In both cases, we can consider the effective coherence lenght $\xi^{-1} = \xi_0^{-1} + l^{-1}$, so that $\xi = l$ and $\xi = \xi_0$ in respectively the dirty and clean limit, at $T = 0$.

Different lenght scales characterizing the superconducting samples can be estimated from standard expressions for superconductors in the dirty limit [63]. The zero temperature penetration depth λ is obtained from

$$\lambda = 1.05 \times 10^{-3} \sqrt{\frac{\rho_N}{T_c}} ,$$

where ρ_N is the normal state resistivity. The BCS coherence length $\xi_{BCS}$is given by

$$\xi_{BCS} = \frac{1.81 \times 10^{-8}}{\sqrt{T_c S}} ,$$

where $S \equiv -\frac{dB_{c2}}{dT}\big|_{T_c}$, the slope of $B_{c2}(T)$ at T_c. The Ginzburg-Landau (GL) coherence length ξ_{GL} is

$$\xi_{GL} = \sqrt{\frac{\Phi_0}{2\pi B_{c2}}} ,$$

where $\Phi_0 = h/2e$, the vortex flux quanta. Finally, the GL parameter κ can be obtained from

$$\kappa = 3.54 \times 10^4 \sqrt{\rho_N S} \, .$$

The values of these lenght scales for some $Fe_xNi_{1-x}Zr_2$ sample are taken from [4], and given in table 5.1 and are found to be typical of strong type-II superconductors.

x	ρ_N ($\mu\Omega$m)	B_{c2} (T)	T_c (K)	S (T/K)	λ (μm)	ξ_{BCS} (nm)	ξ_{GL} (nm)	κ
0	1.3±0.1	4.8±0.1	1.9±0.1**	-2.7±0.2*	0.9	8.1	8.3	66
0.1	1.4±0.1	5.5±0.1	2.72±0.05	-2.7±0.2*	0.8	6.7	7.7	69
0.15	1.5±0.1	4.7±0.1	1.72±0.08	-2.7±0.2	1.0	8.4	8.4	71
0.2	2.1±0.2	3.9±0.1	1.54±0.05	-2.7±0.2*	1.2	8.9	9.2	84
0.3	1.6±0.1	4.0±0.1	1.53±0.01	-2.7±0.2	1.1	8.9	9.0	74
0.33	1.3±0.1	3.6±0.1	1.60±0.03	-2.7±0.2*	1.0	8.7	9.7	66
0.4	2.1±0.1	3.5±0.1	1.43±0.03	-2.7±0.2	1.3	9.2	9.7	84
0.5	0 .8±0.2	1.81±0.01	1.44±0.01	-2.7±0.2*	0.8	9.2	9.8	52

Table 5.1: Superconducting length scales and pamaraters of $Fe_xNi_{1-x}Zr_2$ for different x. ρ_N was measured at room temperature, and the large errors mostly come from measurements of the distance between contacts. *Not measured, the values are assumed to be close enough to other values found. ** Low T_c value due to a high oxygen content in sample.

Structural relaxation

A word should be said about the T_c values found in table 5.1 as they are significantly lower than expected for such materials. For example, for $NiZr_2$, $T_c > 2.8$ K was expected [66]. Moreover, since the introduction of iron is known to supress superconductivity, T_c should linearly decrease with increasing iron content. Instead T_c for $Fe_{0.1}Ni_{0.9}Zr_2$ is higher than for $NiZr_2$. They are two possible explanations for these odd findings [4]. One arises from the facts that the as made ribbons have various state of structural relaxation. An amourphous metal is structurally relaxed when it is heated to a temperature about 50 K below its crystalisation temperature and

is analogous to the annealing of crystals. This was not done in this study beacuse this process makes the samples more brittle, such that they are more susceptible to breakage when soldering of contacts is made, or when it is cooled down. However when the samples are not relaxed, there is a non-uniform distribution of voids, and they might have different amounts of strain fields wich makes them incomparable. Structurally relaxed samples typically show a T_c which is about 10% higher [47], but at least they are comparable.

Another explanation for the lower T_c values found is that the samples could contain an important amount of oxygen, which is know to lower T_c [47]. Much effort was done during sample preparation to prevent oxydation, as we will see in the next section.

5.1.2 Sample preparation

The alloys were prepared by arc-melting the appropriate amounts of high purity Zr (99.95% pure), Fe (99.9% pure) and Ni (99.999% pure), under a Ti- and Zr- gettered prefurified (99.998%) argon gas to avoid oxygen contamination [47]. The alloys ingots were remelted 3-4 times under the same conditions to ensure their homogeneity.

In order to make the metastable amourphous ribbons, the melt-spinning technique was used. The aim of this technique is to supercool the melted alloys, and it necessitates a high cooling rate of about 10^6 K/s in this case. The process is illustrated in figure 5.1. A small ($\sim$1 g) piece of alloy is dropped in a quartz tube with a narrow orifice at one end. The quartz tube is brought into a sealed chamber, above a polished copper wheel. The entire chamber is evacuated then backfilled with $\sim$17 kPa of He to avoid oxidation. A RF generator is used to melt the alloy button, and the molten material is projected out of the orifice with Ar pressure onto the rim of the spinning copper wheel. The latter, driven by a AC motor, has a tangential velocity of $\sim$50 m/s, which allow the melt to cool at the desired rate 10^5–10^6 K/s [47]. The solid ribbon is spun off the wheel and deposited into a collection tube.

The sample produced are about 1 mm wide and 20 μm thick. The amorphous nature of the sample was verified by X-ray diffraction, and confirmed by the absence of Bragg peaks.

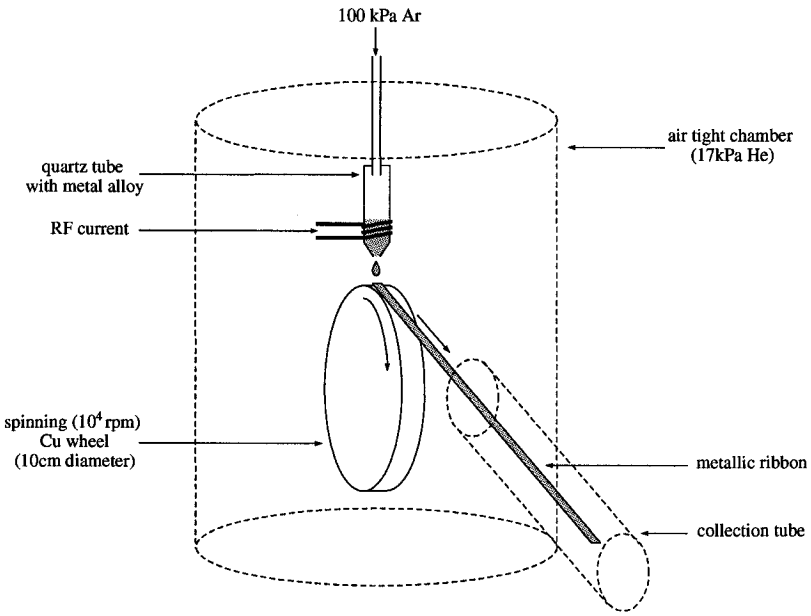

Figure 5.1: Schematic representation of the apparatus used to prepare samples by melt-spinning

5.2 The Helium-3 cryostat

The experiments were performed in a ^{3}He system with a base temperature of 300 mK. A superconducting magnet provided magnetic fields up to 9T. The apparatus is shown schematically in figure 5.2. The sample is placed in the main chamber, which is sealed from the enviroment with a greased cone seal, and brought to high vacuum with a diffusion pump, with a typical base pressure of $\sim 2\times10^{-7}$ mbar at low temperatures. The design is such that the sample is located exactly in the middle of the superconducting coil, and is thus subject to a known and uniform magnetic field.

The principle of operation of the ^{3}He probe is the following. Refer to figure 5.2 for the components name. The probe is brought to liquid helium temperature, 4.2 K, by putting it in a thermally insulated Dewar filled with liquid helium. The 1-K pot fills up with ^{4}He by means of the inlet tube, the opening of which is controlled by a needle valve. By pumping on the 1-K pot with a rotary pump, vaporization of the ^{4}He is induced, and the latent heat associated with the phase transition cools the

probe down to ~1.5 K. Constant cooling power is maintained by a well calibrated needle valve opening, which permits constant resuply of ^{4}He to the 1-K pot, at a sufficiently low rate to prevent heating the 1-K pot to 4.2 K.

At this point, the system is at 1.5 K, and the ^{3}He, lighter than its ^{4}He isotope and with a lower condensation temperature of 3.2 K, has condensed from the ^{3}He reservoir to the ^{3}He pot. By now pumping on the ^{3}He pot, the base temperature of 300 mK can be obtained. This is done in a closed circuit by means of the sorbtion pump. The latter is made of a porous coal-based material, which absorbs gas when cold, and expulses gas when hot. It is cooled to ~4.5 K with cold helium gas from the 1-K pot pumping line, and heated with a resistive heater of nominal power 24 W. At 30 to 70 K, the sorbtion pump expulses all absorbed gaseous ^{3}He which is then condensed in the pot thanks to the cold 1-K pot. By cooling the sorbtion pump one increases the pumping power until it reaches 7 to 4.5 K, where a good equilibrim of pumping versus condensation of ^{3}He is reached, and brings the system to base temperature. At intermediate temperatures of the sorb, the pumping/condensation trade-off is less favorable so that the cooling power is diminished, and the temperature is increased. The temperature is monitored at the ^{3}He pot level with a Lakeshore calibrated Cernox thermometer, and thermalization of the sample and wires is ensured with a high purity (99.999%) copper tubing.

To prevent heat losses, the wires that connect room temperature to the sample are thermally anchored at the ^{3}He pot (300 mK), at the 1-K pot (1.5 K) and near the sorbtion pump at 4.2 K. The wires up to the 1-K pot are made of resistive manganin to limit heat losses, but from the 1-K pot to the sample, wires are in copper to optimize thermalization, and also to limit heating when large currents (0.5–3 mA) are send to the sample. A high vacuum vacuum in the main chamber is always maintained to isolate the system from its surroundings at 4.2 K.

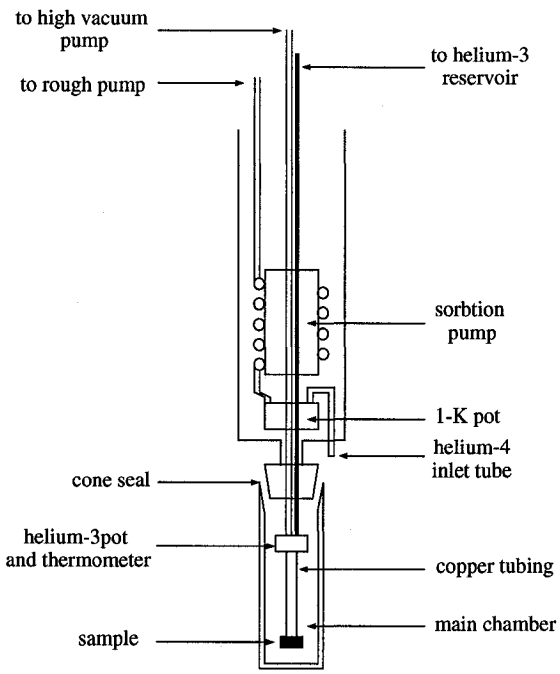

Figure 5.2: Helium-3 system diagram with some internal components

5.3 Thermal conductivity setup

5.3.1 Description

As brefly explained in section 3.1, the method used to measure thermal conductivity is the longitudinal steady state method. In this method, one end of the sample is connected to a thermal ground at a known temperature and then a constant heating power is applied at the other end of the sample. The steady state is reached when the temperature gradient across the sample is constant, and at this point the thermal conductivity is given by

$$\kappa = \frac{\text{power}}{\text{temperature gradient}} \times \text{geometrical factor} .$$

The base temperature need not be perfectly constant. One can do sweeps in temperature, as long as the time constant of the temperature change $\left|\frac{1}{T}\frac{dT}{dt}\right|^{-1}$ is much lower than the response time of the sample and thermometers with respect to a change in temperature.

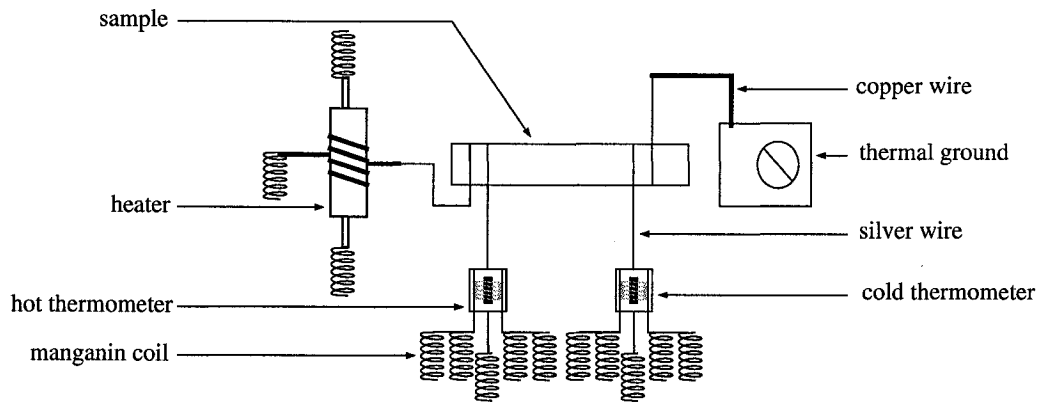

Figure 5.3: Schematic drawing of the thermal conductivity apparatus

The setup is illustrated schematically in figure 5.3. The thermal ground is a ~1 inch diameter copper piece –also the sample holder– clamped to the copper tubing of the ^{3}He system. A 80μm copper wire is clamped to it and is connected with non-superconducting solder to a 50μm silver wire soldered to the sample. Power is supplied by a 10 kΩ ceramic resistor to the sample by means of a 50 μm silver wire, soldered with non-superconducting solder to a 80μm copper wire wound around the resistor and fixed with heat conductive GE 7031 varnish. The ceramic resistor has a very low temperature dependance: at 4.2 K it suffers a change in resistance of about 5% from its 300 K value. It thus supplies a constant power through the temperature range of the experiment. The temperature is measured with two Lakeshore Cernox resistors of 40 Ω. Those thermometers are made of a patented oxide-nitride thin film with Au-Mo contact pads over a 1×1.5 mm^2 sapphire substrate. Good thermal contact with the thermometer is achieved with 50 μm silver wires soldered with non-superconducting solder on the sapphire substrate. Our thermometers have an exponential temperature dependence over the studied temperature range of 0.3 to 3 K and therefore had a good temperature sensitivity. See figure 5.4 for a sample graph of the temperature calibration of the thermometers. Furthermore, 4-probe resistance measurements were possible by using the 2 thermometer connection as the voltage probes, and by using the heater and thermal ground connections as the current contacts.

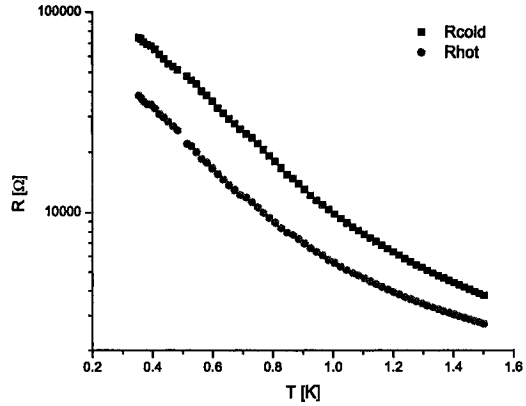

Figure 5.4: Sample temperature calibration of the Cernox resistances from 0.3 to 1.5K. The temperature dependence is close to exponential, and the sensitivity $|\mathrm{d}R/\mathrm{d}T|$ is 200000 Ω/K at 0.3K and 6000Ω/K at 1.5K.

For an accurate measurement of the thermal conductivity, all the heat dissipated by the heater has to go across the sample to the thermal ground. Thus the setup is designed to limit heat losses trought the wires, heater, thermometers, the residual gas in the main chamber or by radiation. Manganin coils ($\sim$75 Ω of 25 μm wire) were used to isolate thermally the thermometers, the voltage and current probes, and heater from the copper sample holder. Of capital importance is the quality of the thermal contacts to the sample and various components (thermometers and heater) that can cause heat losses. See the next section for an estimation of the sources of errors.

5.4 Experimental procedure

In our experiments we used a novel technique to aquire the data for the thermal conductivity measurements. We could not use the standard static steady state method because the temperature of the thermometers were not stable enough even though the temperature of the system remained stable to 0.1%. To counter that effect we decided to perform slow sweeps in the temperature, and this way we were able to

obtain stable and noise-free voltages across the thermometers. In the static steady state method one waits for temperature stabilization, then reads the voltages across the thermometers on the sample and of the calibrated thermometer of the system, to get an in-situ calibration of the sample thermometers. Then power is applied to the heater, which changes the voltage across the sample thermometers. After stabilization of the voltages, they are read and changed to temperature with the calibration points taken over many temperatures, and ΔT is obtained. In this dynamic method however, measurements are taken continuously, and one does not wait for temperature stabilization since it is changing. Therefore current cannot be applied to the heater over long periods of time, and is rather applied alternatively at a frequency $f \sim 1/4\tau$, where τ is the time response to a change in temperature of the sample and thermometer. What we measure is then the dynamic response of the thermometers over the short pulses of heating power. The response of the thermometers being exponential, a program was designed to fit the resistance curves to a simple exponential formula

$$Ae^{-(t-t_0)/\tau} + B \ ,$$

so that even though the time during which the pulse was applied was not sufficient to achieve saturaturation of the thermometer voltages, one could predict it by determination of the coefficient B of the fit, which corresponds to the value of the saturation resistance when $t \to \infty$. Moreover, one could obtain the characteristic time response of the setup with the pamameter τ of the fit. However, although the sweep rate $\left|\frac{1}{T}\frac{\mathrm{d}T}{\mathrm{d}t}\right|^{-1} \approx 5000 \times T$ s, which is much greater than the response time τ of the thermometers and sample (at most 15s at low temperatures: see figure 5.6(a)), the temperature dependence of the thermometers was essentially exponential and therefore suffered significant change over the time range $1/f$ used for the exponential fit. This had little influence on the value of B but gave inconsistent results on the decay time τ. Therefore a linear component in time coresponding to the linear change in temperature was subtracted to the curves before fitting, and added after. See figure 5.5 for an illustration of the fit. The temperature of the system was monitored in parallel, and the program would do the average and standard deviation of

the temperature over each fitting range. The program would then output two curves as a function of temperature for each thermometers: 1) B_0, the saturation resistance when the heater is turned off and 2) B_Q, the saturation resistance when the heater is turned on. One would then use B_0 as the calibration curve: $\log B_0$ was fitted with a high degree polynomial with respect to $\log T$, and the polynomial fit was subsequently used on $\log B_Q$ to obtain the temperature when the heat gradient was present. It is important to do in-situ calibration of the thermometers because one cannot rely on a given calibration: the thermometer resistances would change by some amount over different temperature sweeps. The fits would yield T_{hot} and T_{cold}, the respective temperatures of the "hot" (closer to the heater) thermometer and "cold" thermometer (closer to the thermal ground), and the temperature gradient $\Delta T = T_{hot} - T_{cold}$ can be obtained. Then one obtains the thermal conductivity as a function of the average tempetature $\overline{T} = (T_{hot} + T_{cold})/2$ as

$$\kappa(\overline{T}) = \frac{U \times I}{\Delta T} \times \frac{L}{A} ,$$

where U and I are the voltage across and current passing throught the heater, L the distance between the thermometer leads and A the cross-section area of the sample. It should be noted that it is important that the temperature gradient across the sample is not too large. Indeed, by having $\Delta T/T$ too large one is faced with two problems. The first one is that the average temperature $\overline{T}$ becomes a bad estimate of the actual temperature of the sample, since the local temperature would vary greatly over the lenght of the sample. The second problem is that we might push the system into the non-linear transport regime: ΔT versus the heater power P becomes non linear, and the ratio $P/\Delta T$, the thermal conductance, would *not* be constant at a given temperature but would depend on P. Therefore $\Delta T/T$ is traditionally kept near 10% so that 1) the temperature of the sample is well-defined and 2) the thermal conductivity is independent of P over a whole range. Finally, $\Delta T/T$ must be greater than 5% to have acceptable noise levels.

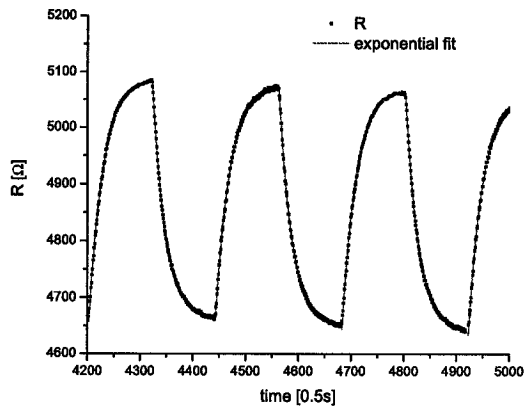

Figure 5.5: Example of an exponential fit done on the data

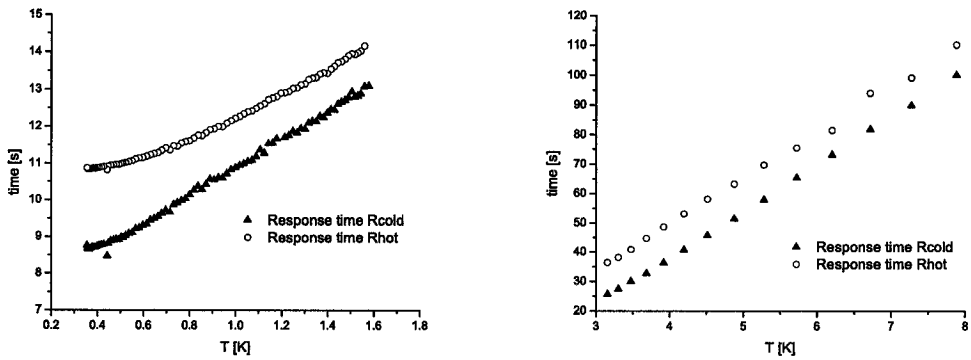

(a) (b)

Figure 5.6: Response time of the thermometers in the thermal conductivity setup as a function of temperature for T between (a) 0.3 and 1.5 K, and (b) 3 and 8 K.

5.4.1 The equipment

A few words should be said about the apparatus used in the data aquisition. The system temperature was monitored by an AC resistance bridge (a Picowatt AVS-47) and controlled with a Picowatt TS-530A PID temperature controller. The sample thermometers were put in series and the voltage across them was measured with two lock-in amplifiers (a SR-850 and SR-830 from Stanford Research Systems) coupled at the same frequency. A lock-in sends a variable frequency AC voltage, which is converted into a current trough a 10MΩ resistor, and like the resitance bridge (which operates at a constant low frequency of 17Hz), only the in-phase voltage at the output frequency is read. Finally, resistance measurements of the sample were made with a 17Hz LR-400 resistance bridge by Linear Research. It provided a continuously variable current source from 0 to 10mA. All the data was monitored and recorded on a computer via a GPIB interface.

5.5 Sources of error

5.5.1 Data analysis

The procedure described in the above section relies on three fits, each one adding a systematic error. The first fit is to subtract a curve to the data prior to the exponential fitting. This curve was obtained by doing an average over the time $2/f$ on the data, so that the positive and negative peaks corresponding to the pulses of the heater would be smoothed out. This result was the best approximation of the temporal behavior of the data and its corresponding error was negligible. The second fit was the exponential fit on τ and B (t_0 was kept fixed to the time of the start of the pulse). The exponential behavior was quite remarkable and led to small errors (less than 1%) on the values. For verification, difference between fit and data was systematically calculated by the program and gave warnings when bad fits occured. Finally, the deviation in the temperature over a fitting range was of typically 1%. The most error came from the polynomial fits used for the calibration: a polynomial

of degree 9 was necessary to keep the error on the temperature calibration below 2%. This was needed especially for the low temperature data points which suffered from unwanted fluctuations from a smooth behavior. The calibration fit was the main source of error for the thermal conductance: an error of 1% on T_{hot} and T_{cold} leads to an error of about 14% in ΔT and on $P/\Delta T$, in the regime when $\Delta T/T = 10\%$.

5.5.2 Sample contacts

The contacts of the thermometers, heater and thermal ground to the sample need to be very good to be certain that thermalization is rapid and lossless. Ideally one can use non-superconducting solder (a eutectic alloy of 82.5% Cd and 17.5% Zn in mass %, with T_c=1–1.6 K) and solder on a large surface so that the thermal conductance of the contact is optimal.

In our case non-superconducting solder could not be used on the Fe-Ni-Zr samples because it has a too high melting temperature around 400 °C, very close the the crystallization temperature of the samples. Its use led to critical modifications of the properties of the samples, observable by a considerable broadening of the superconducting transition. Instead, 99.99% pure In solder was used: while being superconducting below 3.4 K and 28 mT, it has a high thermal conductivity of 2 W/cm·K at 0.3 K [67]. Assuming the solder has the minimal size of a 50μm diameter tube over 1 mm, its thermal conductance at 0.3 K is 0.4 mW/K, four orders of magnitude higher than the thermal conductance of our samples, as seen in the following section. Thermal loss through the contacts are thus negligible.

An important source of error in the thermal conductivity comes from the measurement of the geometric factor L/A (see equation 3.2). One needs to measure the thickness and width of the sample, as well as the distance between the temperature leads. The samples being quite thin around 25 μm, its measurement lead to a considerable uncertainty of 20%. There is however a larger uncertainty in the distance between the leads on the sample. Each contact was at most 0.3mm wide, and being around 3.5 mm apart, the uncertainty on L is easily 15%. Thus the combined error on the geometric factor induces a systematic error on the thermal conductivity between

20 and 30%. Considering the already large systematic error of at least 10% induced in the data analysis, we chose not to consider the geometric factor in our results as this would have dramatically increased the total error.

5.5.3 Estimation of heat losses

The thermal conductivity of the Fe-Ni-Zr glassy metals is rather low, and special care must be taken to avoid significant heat losses that would affect the measurements. Point 2 and 3 are taken from the book by G.K. White [68], and found in the thesis of Lussier [69] and Lambert [70].

1. *Losses trough the wires.* In the steady state (after ~60 s in our experiments), the heat coming from the heater has dissipated through the sample and thermometers, but also some heat is constantly drained through the measuring wires. It is important that this loss is minimal. To estimate it we need the values of absolute thermal conductance of the manganin wires and of our sample. From 1 to 4 K, the thermal conductivity of manganin is given by $\kappa = 0.94T^{1.2}$ mW/(cm·K) [67]. We can extrapolate this relation to 0.3 K where it should be .22 mW/(cm·K). At 3 K it is 3.5 mW/(cm·K). The values of the thermal conductivity of amorphous superconductors ($Zr_{0.7}Pd_{0.3}$, T_c=2.53K [56] and $Mg_{0.7}Zn_{0.3}$, T_c=0.11K [71]) found in the litterature are around 10^{-4} W/(cm·K) at 0.3 K and 10^{-3} W/(cm·K) at 3 K. Our samples have a cross sectional area of around 1×0.025 mm^2 and are 5 mm long, and therefore should have a thermal conductance of approximately 5×10^{-8} W/K at 0.3 K and 5×10^{-7} W/K at 3K. In contrast our manganin wire has a 25 μm diameter and is 10 cm long, so that it has a thermal conductance of 10^{-10} W/K at 0.3 K and 2×10^{-9} at 3K, 2 orders of magnitude lower than that of our samples.

2. *Losses through the surrounding gas.* A good vacuum must be maintained in the chamber to prevent heat with the residual gas exchange between the components of the system that have different temperatures. According to [68], the power

loss by conduction trough the residual gas is given by

$$Q = \frac{\text{constant}}{\sqrt{T}} \times a_0 p(T_2 - T_1) \text{ W/m}^2 ,$$

where p is the pressure of the gas, T_1 and T_2 the temperatures of the two points between which heat is exchanged, and a_0, called the accomodation coefficient, is always smaller than unity. In air at room temperature, the factor constant/$\sqrt{T} \simeq 1.2$, and can thus be approximated to 12 (38) at 3 K (0.3 K). The vacuum being maintained at 2×10^{-7} mbar, the constant heat exchange between the system and the liquid helium outside the chamber at 0.3 K is thus $Q < 3.0$ mW/m^2. Considering the surface (0.012 m^2: 1 inch diameter and 15 cm long) of the chamber, the power loss is less than 36 μW. In comparison, since typical heating used to sweep or control temperature was in the 100 μW range at its lowest, the cooling power of the system is around 100 μW. This would imply considerable loss, however stable system temperature were easily achieved. Also to be considered is the power dissipated from the heater to the thermal ground. In our experiments, at 0.3 K, the difference in temperature between the hot thermometer and the thermal ground was around 0.06 K so that the difference between the heater and the thermal ground is estimated around 0.08 K, which leads to a $Q < 61$ μW/m^2. The heater having a surface of 4×2 mm^2, the power loss is less than 0.5 nW, 5% of the typical 10 nW used in thermal conductivity measurements. This is an upper bound to the loss, but at least 1% error is expected to occur due to this phenomenon.

3. *Losses by Radiation.* The heat transfert by radiation follows a T^4 law and therefore is present only at high temperatures. For two plane parallel surfaces of emissivities ϵ_1 and ϵ_2 at respective temperatures T_1 and T_2, the heat transfert by radiation from an area A per unit time is given by [68]

$$\dot{Q} = \sigma_S A[T_2^4 - T_1^4] \frac{\epsilon_1 \epsilon_2}{\epsilon_1 + \epsilon_2 - \epsilon_1 \epsilon_2} ,$$

where σ_S is Stephan's constant, $\sigma_S = 5.67 \times 10^{-8}$ W/m^2/K^4. In the worse case scenario, we asume both emissivities are equal to unity. The radiation from

the outside of the chamber of area 0.012 m^2 at 4.2 K to the system leads to a $\dot{Q} = 0.2$ μW at 0.3 K and of $\dot{Q} = 0.1$ μW at 3 K, in both cases much less than the cooling power of about 100 μW at 0.3 K and 100 mW at 3 K of the system. Now the power loss due to radiation between the base at $T_1 = 0.3$ K and the heater at $T_2 = 0.3 + 0.08$ K is $\dot{Q} = 6$ pW!, using $A = 6$ mm^2. Radiation is not a problem at low temperatures.

Chapter 6

Results and Discussions

In this section we describe qualitatively the results obtained for resistance, magnetoresistance, and thermal conductance of the $Fe_{0.5}Ni_{0.5}Zr_2$ sample. Resistance measurements were done by Josianne Lefebvre at the base temperature of 300 mK, and up to fields of 3 T, where the peak effect is observed. Preliminary results on the thermal conductance are shown, on the temperature range of 0.3 to 1.5 K, and under a field of 7.5 T.

6.1 Longitudinal resistance and the peak effect

6.1.1 Critical temperature

The critical temperature T_c was measured in controlled slow sweeps in temperature, without a magnetic field and with a current $I = 100$ μA; see figure 6.1. A small hysteresis in temperature is observed, and is due to a non-perfect thermalization of the sample with the thermal ground (a different setup of the one for thermal conductivity was used), and adds to the error of $T_c = 1.44 \pm 0.01$ K. The transition is very sharp, with a small width of 30 mK between 90 and 10% of the normal state value, and indication of a homogeneous and pure sample.

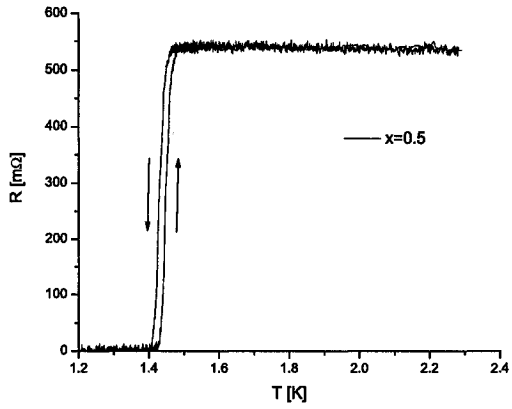

Figure 6.1: Resistance as a function of temperature for the $Fe_{0.5}Ni_{0.5}Zr_2$ sample. A current of 100 μA is used and a small hysteresis is observed, with the direction of temperature change indicated by the arrows. A sharp superconducting transition is found at 1.44 K

6.1.2 The peak effect

The magnetoresistance of a $Fe_{0.5}Ni_{0.5}Zr_2$ sample with a driving current of 0.5 mA is shown in figure 6.2(a). It is a magnificent example a strong peak effect, where pinning is sufficient to induce an almost reentrant superconducting phase. The different phases are depicted in figure 6.2(b) for the B-down sweep and their description follows.

The first depinning phase

The first depinning phase starts at the first critical field H_{c1} when the sample departs from the zero resistance superconducting phase. The transition is defined to happen when the resistance exceeds 0.5 mΩ, our experimental resolution (a combination of random noise and systematic instrumental error), at $H_{c1} = 0.16 \pm 0.04$ T. At this point vortices are present in the superconductor, and the current acts as a driving force which puts them into motion, thereby creating a finite resistance across the sample. This phase is generally described as the ordered moving Bragg glass [17, 4], characterized by weakly pinned vortices. It is qualitatively similar to the flux-flow regime, with a resistance linear in B, although with a proportionality coefficient smaller than the Bardeen-Stephen one of R_N/B_{c2}.

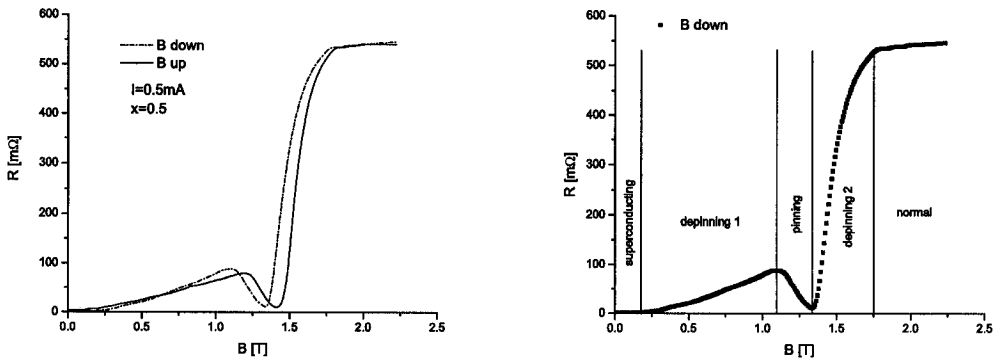

(a) (b)

Figure 6.2: (a) Magnetoresistance of the $Fe_{0.5}Ni_{0.5}Zr_2$ sample showing the peak effect in an up and down sweep (at a sweep rate of 0.015 T/s) at 0.3 K and with a driving current of 0.5 mA (b) Illustration of the various vortex phases in the B down sweep.

The reentrant pinning phase

The reentrant pinning phase is defined to occur at the field when dR/dB=0, at 1.10 $\pm$ 0.08 T in this case, and is characterized by a sudden decrease in the resistance: the peak effect. This pinning is quite drastic in the $Fe_{0.5}Ni_{0.5}Zr_2$ sample, bringing the sample to an almost zero resistance superconducting state, with a small residual resistance of 2% (11 mΩ) of the normal state resistance value. This is the first observation of such a strong reentrant behavior in a amorphous superconductor, and it is also seen in other samples with different concentrations of Fe/Ni [4]. As discussed in section 2.4.2, this effect is now attributed to a softening of the vortex lattice (LO theory) due to an order-disorder phase transition which occurs when the distance between vortices, tuned by the external field, is of the order of ξ, so that inter-vortex correlations become strong.

The second depinning phase

The second depinning phase occurs when the resistance departs from its minimum value, at 1.327 $\pm$ 0.007 T in this case, and is characterized by a abrupt increase in

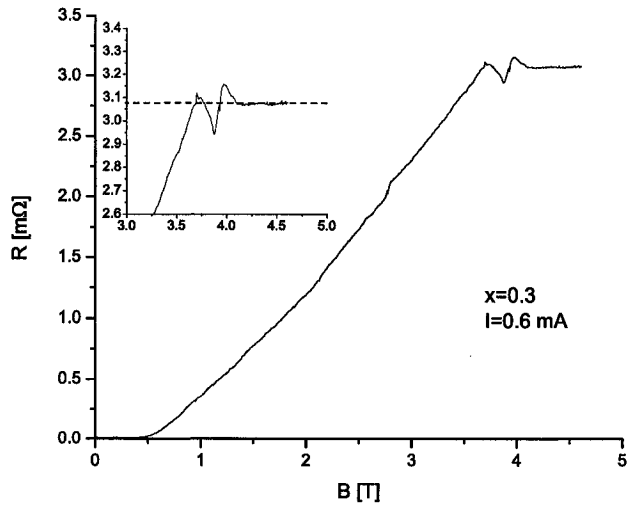

Figure 6.3: An anomalous overshoot in the vortex-flow resistance in $Fe_{0.3}Ni_{0.7}Zr_2$. The temperature is 0.8 K and the driving current is 0.6 mA.

resistance up to $B_{c2} = 1.805 \pm 0.007$ T (the point of highest negative curvature) where the sample becomes normal. The vortex dynamics in this phase are very different from the moving Bragg phase found in the depinning 1 phase: it is described by a smectic or plastic motion of vortices [17, 4].

6.1.3 An inhomogeneous superconducting phase

We present here some magnetoresistance data taken in the vortex phase of $Fe_{0.3}Ni_{0.7}Zr_2$. In this experiment, the sample was microstructured, *i.e.* the distance between the voltage contacts was kept as small as possible, so that the total area between the contacts was around $50\mu m \times 100\mu m$. What we observed in such a configuration was an unexpected and anomalous overshoot of the vortex-flow resistance around the upper critical field, of about 3 and 1.5 % higher than normal state resistance. See figure 6.3.

This effect was observed at different driving currents and temperatures (see figure 6.4) and also on a similarly microstructured $Fe_{0.2}Ni_{0.8}Zr_2$ sample. It is quite perplexing, as it implies that the resistance is bigger in the superconducting state than in the normal state. This effect has to the best of our knowledge never been observed. We

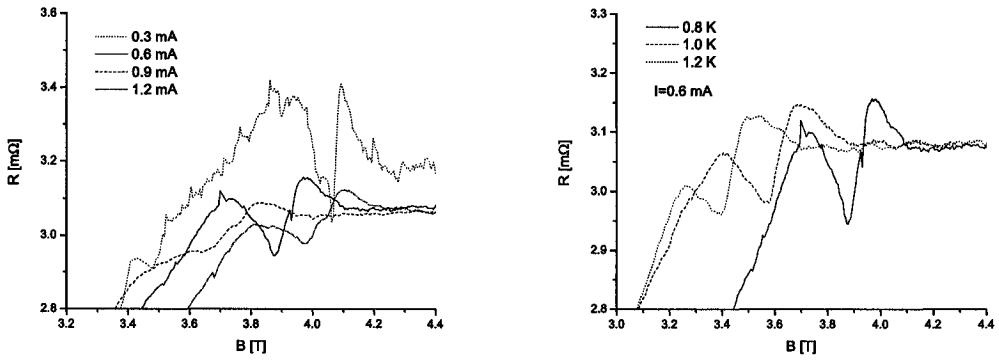

(a) (b)

Figure 6.4: Anomalous overshoot near B_{c2} in $Fe_{0.2}Ni_{0.8}Zr_2$ for (a) various driving currents at 0.8 K , and (b) different temperatures at 0.6 mA

theorize it is due to the inhomogeneity of the superconducting phase: by assuming the bulk of the sample is normal while only localized parts of it are superconducting, such behavior can be predicted. We can imagine a sample of size $l \times L$ with a normal region of size $r^2 L \cdot l$, as illustrated schematically in figure 6.5.

Now we can consider every of the nine regions in figure 6.5 separated by dotted lines as separate resistors, attributing to the superconducting regions of size $a \times b$ the Bardeen-Stephen vortex-flow resistance $R = R_N \frac{B}{B_{c2}} \frac{a}{b}$ and to the normal region the resistance R_N. We then simply calculate the total resistance of the resistor network. The results are given in figure 6.6 for different values of r. We can see that for large normal regions (large r), we are able to mimic an overshoot behavior. It would thus be plausible to attribute the overshoot phenonemon to inhomogenities in the sample. However, it should be noted that this model is very simple, and almost undersophisticated: it must only serve as a guideline. As outlined in the following sections, the best way to detect bulk superconductivity is through thermodynamic probing, by measuring for example heat capacity or magnetization. The size of the discontinous step across the superconducting phase transition is then a direct measure of the size of the sample which actually is superconducting: bulk (edge) superconductivity implies

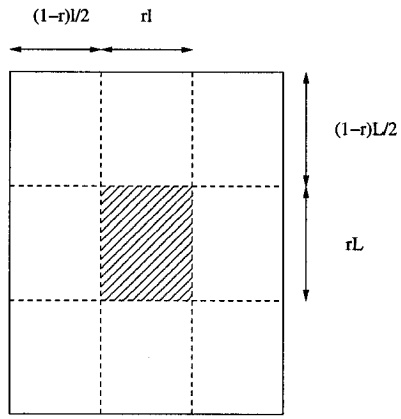

Figure 6.5: Simple model of an inhomogeneous sample with some normal and superconducting regions.

a large (small) jump in heat capacity or magnetization.

6.2 Thermal conductance

We present in this section our preliminary results on the thermal conductance of $Fe_{0.5}Ni_{0.5}Zr_2$. We were faced with many problems in trying to make the measurements and this is certainly reflected in the quality of the data. Firstly, it was quite difficult to take data at temperatures higher than 1.5 K, the temperature of the 1-K pot. This is because by heating the system from the helium-3 pot (where the heater is located), one would totally evaporate the ^{3}He in reaching say 3 K. But the ^{3}He would then recondense, the sorbtion pump being at 25 K (this was needed to reach 1.5 K), thus creating a thermal link to the 1-K pot at 1.5 K, which made the system difficult to control. The only way to do high temperature sweeps was to heat and keep the system near 10 K, and letting the sorbtion pump cool down, thus trapping the ^{3}He in the sorbtion pump. This way the system would be slowly cooled with the 1-K pot, without the ^{3}He serving as an exchange gas. The downside is that this method would bring the system to 1.5 K in an enormously long time, in around 20h, which is quite inefficient. Therefore we could not do many high temperature sweeps, and this prevented us from having precious calibration of the thermometers above 1.5 K.

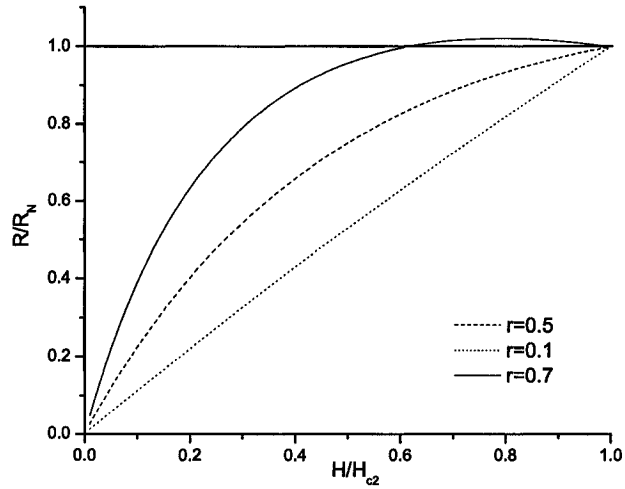

Figure 6.6: Normalized resistance of a simple resistor network modelizing an inhomogenous sample composed of normal and superconducting regions

This in turn lead to larger errors and large unphysical fluctuations in the thermal conductance near 1.5 K as we were missing calibration points for the thermometers.

Secondly, the Cernox thermometers used in our setup suffered from large variation in calibration over small thermal cycles and under a magnetic field, as seen in figure 6.7. Although one is expected to observe small variation over thermal cycles and under a magnetic field, in our case the calibration could vary of 50% over *subsequent* sweeps between 1.5 and 0.3 K. Even though calibration variations are absorbed in making *in-situ* calibrations for each sweeps, nevertheless this poor reproducibility is reflected in our results.

6.2.1 Nonlinear transport

One challenge in doing thermal conductivity measurements is to determine the power P to apply to the sample. By applying too much power one can drive the system into the non-linear transport regime, where thermal conductivity depends on P, and by applying too little power the signal difference between P applied and non-applied becomes too small compared to noise levels. Also, traditionally one chooses P so

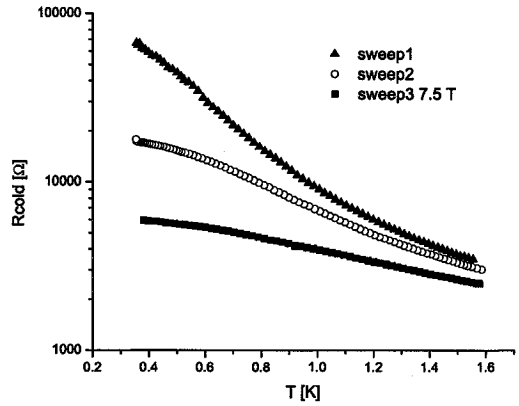

Figure 6.7: Calibration reproducibility of the cold Cernox thermometer over small thermal cycles and under a magnetic field. The variation is higher than 50%.

that $\Delta T/T \sim 10\%$, so that one can use the average temperature of the hot and cold thermometers as the sample temperature without unwanted effects. The explanation (taken from [28]) follows. Assume that the thermal conductivity is given by $\kappa = \alpha T^3$, and that the temperature difference along the sample is ΔT. The heat flow is then

$$\int_T^{T+\Delta T} \kappa \mathrm{d}T = \alpha \int_T^{T+\Delta T} T^3 \mathrm{d}T = \frac{1}{4}\alpha\Big[(T+\Delta T)^4 - T^4\Big] \,. \tag{6.1}$$

The thermal conductivity is then given by equation 6.1 divided by ΔT, assuming a unit geometric factor. Now the mean temperature of the sample is given by $T+\Delta T/2$, and at this temperature the true conductivity is $\alpha(T+\Delta T/2)^3$. Neglecting high order ΔT terms, the difference between these expressions is $\Delta\kappa \approx T(\Delta T)^2/4$, and we obtain

$$\frac{\Delta\kappa}{\kappa} \approx \frac{1}{4}\Big(\frac{\Delta T}{T}\Big)^2 \,,$$

so that by having $\Delta T/T = 10\%$, the percent difference between the apparent and true conductivities is only 0.25%. One can use the same reasoning when $\kappa \propto T^2$ and it gives a smaller $\Delta\kappa/\kappa = 1/12(\Delta T/T)^2$, while when the relation is linear the difference between apparent and true conductivities is zero.

We used on the $Fe_{0.5}Ni_{0.5}Zr_2$ sample various heater power values over different sweeps to test the linearity of transport. The results for low temperatures are shown in figure 6.8(a) and 6.8(b). We can see that even by having $\Delta T/T = 45\%$ at 1.4

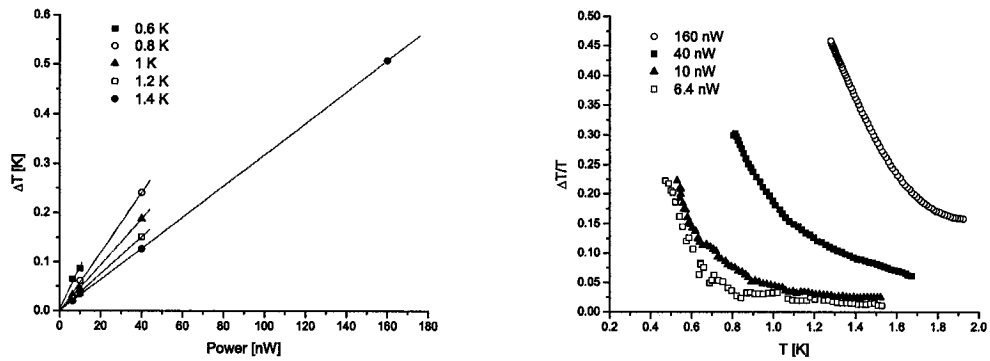

(a) (b)

Figure 6.8: Linearity of thermal transport in the $Fe_{0.5}Ni_{0.5}Zr_2$ sample at low temperatures (a) ΔT versus P curves at different temperatures. (b) $\Delta T/T$ versus temperature for various heater power values.

K the $\Delta T(P)$ curve is very linear. Similarly, having $\Delta T/T = 25\%$ at 1 K or 0.6 K brings no unwanted effects in the thermal transport. We thus can deduce that any power between 40 nW and 10 nW is a good candidate for the studied temperature range. Using 6.4 nW brings higher noise levels while 160 nW elevates too much the temperature of the sample.

At high temperatures, we can see from figure 6.9(a) and 6.9(b) that using 1 μW between 4 and 5 K brings non-linear effects. Indeed, the $\Delta T(P)$ curve is non linear, even at a relatively small temperature gradient of $\Delta T/T = 20\%$. Using 160 nW at $\Delta T/T < 10\%$ is however acceptable. We can clearly see the the power dependance of thermal conductance in figure 6.10.

6.2.2 Three terminal probing

We can deduce useful information by looking into three terminal probing, *i.e* by using the information from individual thermometers. We can calculate the elevation in temperature of the sample when a heat current is applied, at the two location of the thermometers leads. We can further deduce the elevation in temperature at

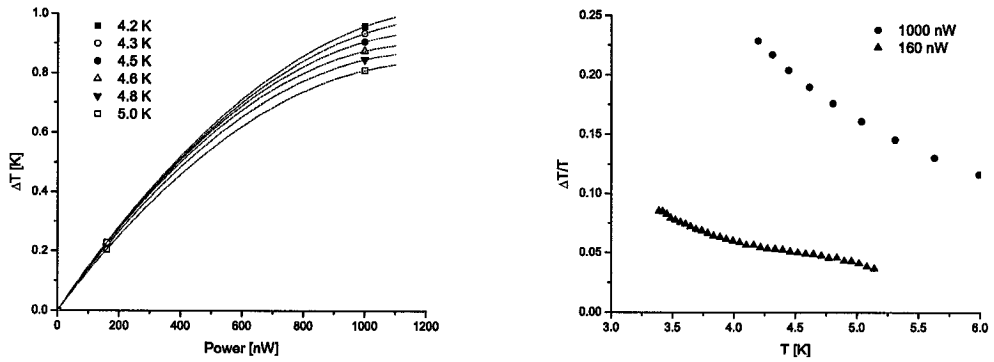

(a) (b)

Figure 6.9: Linearity of thermal transport in the $Fe_{0.5}Ni_{0.5}Zr_2$ sample at high temperatures. (a) ΔT versus P curves at different temperatures. (b) $\Delta T/T$ versus temperature for various heater power values.

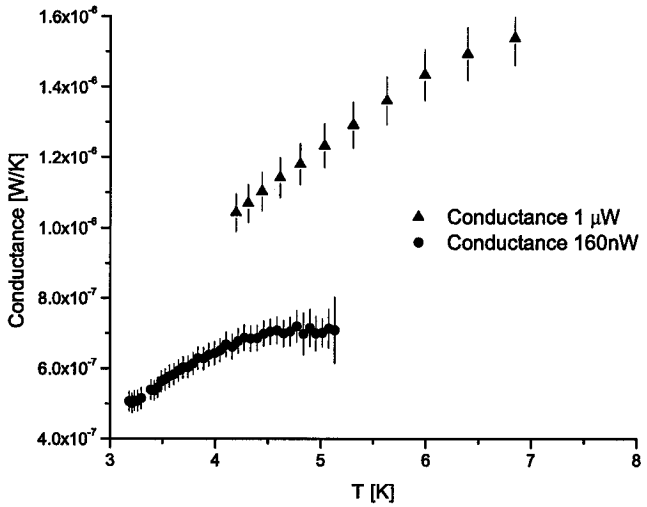

Figure 6.10: Power dependence of thermal conductance in $Fe_{0.5}Ni_{0.5}Zr_2$ at high temperatures. Note the curved behavior of the 160 nW thermal conductance (triangles) near 5 K. It is a calculation artefact due to missing calibration points at those temperature.

any location of the sample by using the values of conductance of the material. Of particular interest is the elevation in temperature at the extreme end of the sample where it is connected to the thermal ground of the setup: by calculating it we can deduce the thermal conductance of the thermal link between the sample and the ^{3}He pot. Indeed, the temperature of the sample before power is applied is that of the ^{3}He pot, denoted by T_s, and equal to the temperature of the hot (cold) thermometer when no power is applied, $T_{hot}(0)$ ($T_{cold}(0)$). We have

$$T_{hot}(Q) - T_G(Q) = \frac{P}{\kappa}\frac{l}{A} = \frac{P}{K\frac{A}{L}}\frac{A}{l} = \frac{P}{K}\frac{l}{L} ,$$

where $T_{hot}(Q)$ and $T_G(Q)$ are respectively the temperatures at the location of the hot thermometer and the thermal ground contact in the presence of a heat gradient. The value of K is the conductance in the four terminal configuration as measured in this work, and L and l are respectively the distances between the hot and cold thermometers and between the hot thermometer and thermal ground. The ratio $l/L = 1.3 \pm 0.2$. Therefore we obtain

$$T_G(Q) - T_s = T_{hot}(Q) - T_s - \frac{P}{K}\frac{l}{L} .$$

We present the results in figure 6.11, using the values of conductances described in the next section. We can see that the elevation in temperature on the sample is at its highest closer to the heater and decreases over the lenght of the sample, as expected from the finite thermal conductivity. Now by calculating $K' = \frac{P}{T_G(Q)-T_s}$, we can obtain an estimate of the thermal conductance of the thermal link between the sample and the cryostat, which in our case is a silver wire plus a copper wire plus a large copper piece. The results are shown in figure 6.12. We can see a large error at higher temperature and non-linearity of transport: it is a rather crude estimate of the conductance. However at low temperatures the deviation is minimal, and at 0.4 K we have a conductance of approximately 2.5×10^{-7} W/K. Considering the weakest thermal link to the cryostat, that is the 50 μm diameter silver wire, with a geometric factor $G \approx 0.64/(0.0025^2\pi) \approx 32000$ cm^{-1}, we obtain an estimate of the thermal conductivity of silver at 0.4 K of 8×10^{-3} W/K·cm. This is within an

acceptable range –20%– considering the crude estimation of the accepted value of 4×10^{-2} W/K·cm found in [67], and therefore an indication that our setup is well thermally grounded.

6.2.3 Phonon and electron contributions

In solids, electrons and phonons are the main contributors to the thermal conductivity, but their individual contributions can in the general case be difficult to distinguish. As we have seen in chapter 3 and 4, the electronic contribution to the thermal conductivity is linear in T, while the phonon contribution to the thermal conductivity in amorphous solids is quadratic in T. Furthermore, in the superconducting state, the population of normal electrons exponentially decreases away from T_c as they are replaced by Cooper pairs. Therefore in superconductors, the principal heat carriers are phonons and if electrons still contribute to the thermal conductivity , it can only be detected a very low temperatures where the phonon contribution also goes to zero.

In a superconducting amorphous metal, one thus expects to have a dominant electronic contribution in the normal state, while in the superconducting state, one expects to see the phonons dominate with a characteristic T^2 dependence attributable to two levels systems. This scenario was readily observed in a superconducting amorphous metal ($Zr_{0.7}Pd_{0.3}$, $T_c = 2.53$ K) by Graebner et. al. [56]. It should be noted that they find a thermal conductivity of 9×10^{-4} W/cm·K at 1 K. As seen in figures 6.13 and 6.15(a), we find a thermal conductance of 2×10^{-7} W/K at 1 K for our sample, and considering our geometric factor $L/A \approx 0.33/(0.002 \times 0.080) = 2000 \pm 600$ cm^{-1}, the thermal conductivity of the $Fe_{0.5}Ni_{0.5}Zr_2$ sample is approximately 4×10^{-4} W/cm·K at 1 K, within a reasonable range of the expected value.

A first test is to look for any difference between the low temperature thermal conductance of $Fe_{0.5}Ni_{0.5}Zr_2$ in the normal and superconducting state. This is simply done by applying a magnetic field higher than $B_{c2} = 1.8$ T. The results are shown in figure 6.13. Although there is some scatter in the data and 20% error, it is evident that the thermal conductance in the normal and superconducting states are very similar quantitatively. At first sight it can only be explained in the following way. In this

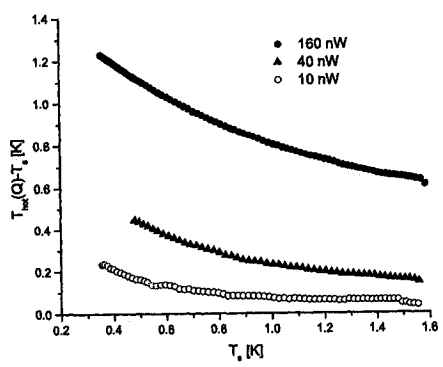

(a)

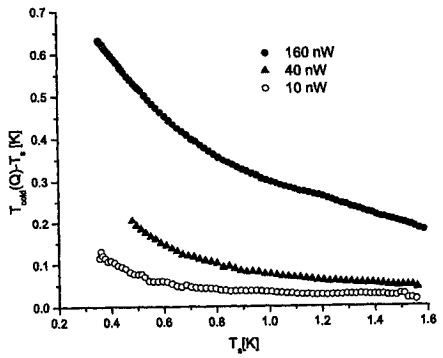

(b)

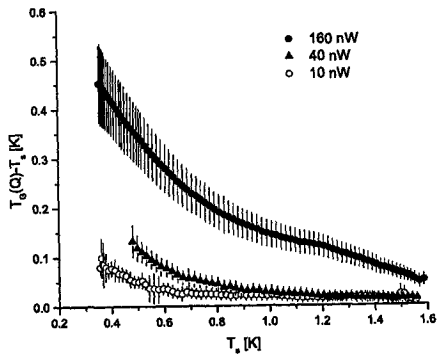

(c)

Figure 6.11: Elevation in temperature for various heater power at the locations on the sample of (a) the hot thermometer, (b) the cold thermometer and (c) the thermal ground contact.

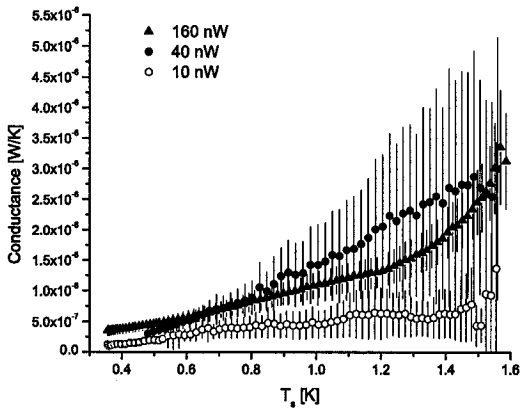

Figure 6.12: Estimated thermal conductance of the thermal link between the sample and ^{3}He for different powers.

disordered material, the phonon contribution to the thermal conductivity is dominant above $T_c = 1.44$ K so that the difference between the superconducting state with no electrons and the normal state with electrons and phonons is minimal. However it seems this hypothesis is improbable as the material is disordered but metallic, and thus should have an important electronic component in thermal transport, linear in T, at least above T_c. Such behavior was reported in [56] and is also seen in our $Fe_{0.5}Ni_{0.5}Zr_2$ sample were thermal conductance behaves quasi linearly as $T^{0.98\pm0.09}$ between 3 and 4 K (see figure 6.14). Therefore, if the main contributors to thermal transport above T_c are electrons, and that we observe no difference between the normal and superconducting state thermal conductance below T_c because of a zero field dependence, the electrons are also to be the dominant heat carriers in the superconducting state. In fact, we observe that $\kappa \propto T^{1.14\pm0.03}$ (figure 6.15(a)) and $\kappa \propto T^{1.3\pm0.2}$ (figure 6.15(b)). This is in apparent contradiction from the fact that electrons are absent in the superconducting phase, that is *if* the material is superconducting in the bulk. However if the sample is inhomogeneous, *i.e.* the bulk of $Fe_{0.5}Ni_{0.5}Zr_2$ would be normal while only parts of the sample are superconducting, one would expect to see a metallic linear thermal conductivity across the superconducting transition as observed in this sample. Evidence for such behavior was suggested in section 6.1.3

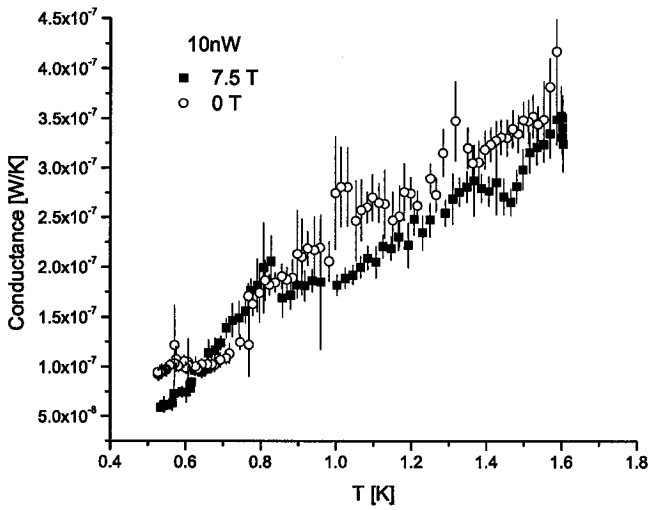

Figure 6.13: Thermal conductivity of $Fe_{0.5}Ni_{0.5}Zr_2$ in zero field and in a field a 7.5 T at low temperatures. The dependence is very similar and the difference is small.

for $Fe_{0.3}Ni_{0.7}Zr_2$. This theory remains to be proven, however. Indeed, as we can see in section 6.1.1, the superconducting transition is very sharp, a reasonable indication of the homogeneity of the sample, in other words of bulk superconductivity. But the best way to test superconducting homogeneity remains by thermodynamic probing such as magnetization M or heat capacity C, where the size of the jump in M or C associated with the second order superconducting phase transition is representative of the size of the superconducting phase in the sample. A large jump in C means that most of the sample became superconducting, and is reflected in κ by a discontinuity at T_c, the latter being the integral of C. A small jump in C however would imply no discontinuity in κ at T_c, as seen in this $Fe_{0.5}Ni_{0.5}Zr_2$ sample.

It is however difficult to draw a definite conclusion of the behavior of thermal conductivity or on the homogeneity of the superconducting phase in this sample. First of all, the data on the thermal conductance presented in this thesis is on a rather limited temperature range, of less than one order of magnitude, and suffers from some unwanted noise. Measurements need to be taken at higher temperatures in order to see the general behavior of the thermal conductivity of $Fe_0.5Ni_0.5Zr_2$, so that

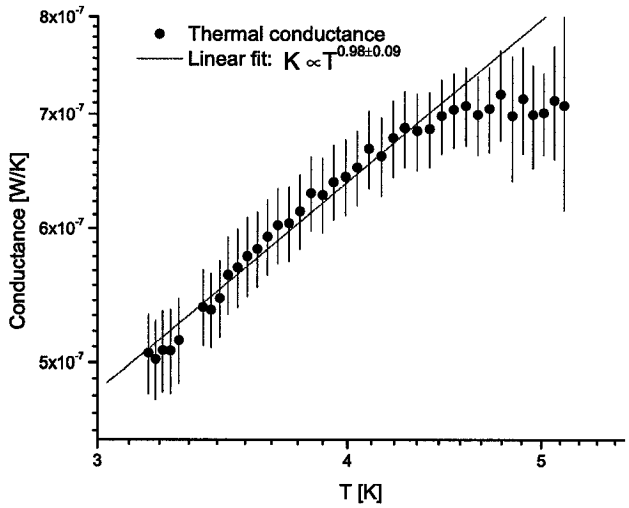

Figure 6.14: Thermal conductance for the superconducting disordered metal $Fe_{0.5}Ni_{0.5}Zr_2$ at high temperatures. We observe a quasi linear dependence $T^{0.98\pm0.09}$ due to electrons. We did not consider the points near 5 K in the fit: the curvature in this region is due to missing calibration point and is not physical.

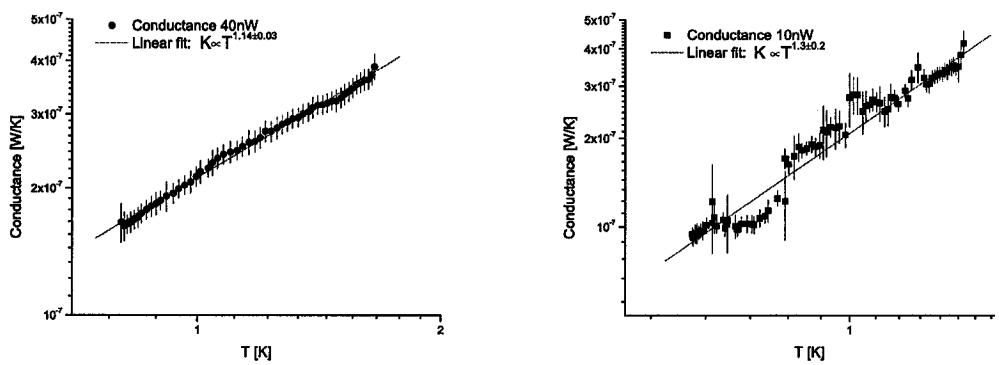

(a) (b)

Figure 6.15: Temperature dependence of thermal conductance for the superconducting disordered metal $Fe_{0.5}Ni_{0.5}Zr_2$ for (a) a heater power of 40 nW, where we have a $T^{0.98\pm0.09}$ behavior, and for (b) a heater power of 10 nW, where we have a $T^{1.33\pm0.2}$ behavior.

one can see to what extent the observed linear behavior due to electrons is dominant and when the phonons start to come into play. Furthermore, in order to measure more quantitatively the composition in the bulk of the samples, one need to use more powerful tools, such as heat capacity or magnetization.

Chapter 7

Conclusion

In this study we have made measurements on the thermal conductivity of the amorphous metallic superconductor $Fe_{0.5}Ni_{0.5}Zr_2$ in the temperature range of 0.3 to 1.5 K and under a magnetic field of 7.5 T well above B_{c2}.

The tests we have made seem to indicate an unexpected dominant electronic contribution to the thermal conductivity in both the normal and superconducting phases. Namely, below T_c we have observed no difference between the thermal conductivity in the normal state (with an applied field of 7.5 T> B_{c2}) and in the superconducting state, and have observed a quasi-linear temperature dependence $\kappa \propto T^{1.14\pm0.03}$ below T_c. A linear term in the thermal conductivity is expected above T_c for a metallic glass as reported in the literature, but normally below T_c electrons condense into Cooper pairs that do not carry heat. Therefore one usually should observe below T_c a characteristic T^2 dependence attributable to phonons in two-level systems found in amorphous solids.

These findings thus suggest that normal electrons are still the principal heat carriers below T_c, and could be an indication of a inhomogeneous sample composed of a bulk normal metallic glass with localized superconducting parts. However we need to test the thermal conductivity in a much larger temperature range to explore the behavior of the thermal conductivity well above T_c to understand when the phonons start to come in play. Furthermore, a thermodynamic study of $Fe_{0.5}Ni_{0.5}Zr_2$ would provide essential information about the bulk properties of those materials: the size of

the jump observed in magnetization or heat capacity associated to the superconducting phase transition is representative of the size of the sample which actually becomes superconducting. Such studies would shine more light on the mechanism involved.

All in all, the Fe-Ni-Zr alloys are fantastic a system to study. As we have seen, they have a very interesting superconducting properties, especially in a magnetic field. They have a very low depinning current, which makes them ideal testbeds for the study of vortex dynamics. In addition, these alloys exhibit the peak effect, and display very diverse vortex phases. A natural extension of this work would be to study the vortex contribution to the thermal conductivity. The vortices being displaced fairly easily in those alloys, we would expect that a reasonably small temperature gradient would be sufficient to displace them across the length of a sample (thus inducing Hall resistance) and contribute to the thermal conductivity to some extent. We can speculate to see an effect analogous to the peak effect, observed in longitudinal resistance with an electrical current, but in Hall resistance with a heat current.

Bibliography

[1] H. K. Onnes, Leiden Comm. **88**, 120b, 122b, 124c (1911).

[2] R. Laughlin, Phys. Rev. Lett. **50**, 1395 (1983).

[3] M. Hilke, S. Reid, R. Gagnon, and Z. Altounian, Phys. Rev. Lett. **91**, 127004 (2003).

[4] J. Lefebvre, Master's thesis, McGill University, 2004.

[5] W. Anderson, B. Halperin, and C. Varma, Philos. Mag. **25**, 1 (1972).

[6] W. Phillips, J. Low. Temp. Phys. **7**, 123 (1972).

[7] V. Z. Kresin and S. A. Wolf, *Fundamentals of Superconductivity* (Plenum Press, New York, 1990).

[8] M. Tinkham, *Introduction to Superconductivity* (McGraw-Hill, New York, 1975).

[9] W. Meissner and R. Ochsenfeld, Naturwissenschaffen **21**, 787 (1933).

[10] E. Maxwell, Phys. Rev. **78**, 477 (1950).

[11] W. W. C.A. Reynolds, B. Serin and L. Nesbitt, Phys. Rev. **78**, 487 (1950).

[12] L. N. Cooper, Phys. Rev. **104**, 1189 (1956).

[13] F. and H. London, Proc. Roy. Soc. (London) **A149**, 71 (1935).

[14] A. B. Pippard, Proc. Roy. Soc. (London) **A216**, 547 (1953).

[15] J. M. Ziman, *Principles of the Theory of Solids* (Cambridge, New York, 1964).

[16] A. A. Abrikosov, Soviet Phys. –JETP **5**, 1174 (1957).

[17] T. Giamarchi and P. LeDoussal, Phys. Rev. B **57**, 11356 (1998).

[18] T. Klein *et al.*, Nature **413**, 404 (2001).

[19] A. Pippard, Philos. Mag. **19**, 220 (1969).

[20] A. Larkin and Y. Ovchinnikov, J. Low Temp. Phys. **34**, 109 (1979).

[21] X. Ling *et al.*, Phys. Rev. Lett. **86**, 712 (2001).

[22] T. Giamarchi and S. Bhattacharya, *High Magnetic Fields: Applications in Condensed Matter Physics and Spectroscopy* (Springer-Verlag, Berlin, 2002).

[23] W. Kwok *et al.*, Phys. Rev. Lett. **72**, 1088 (1994).

[24] G. Blatter *et al.*, Rev. Mod. Phys. **66**, 1125 (1994).

[25] K. Ghosh *et al.*, Phys. Rev. Lett. **76**, 4600 (1996).

[26] Y. Paltiel *et al.*, Phys. Rev. Lett. **85**, 3712 (2000).

[27] Y. Paltiel *et al.*, Nature **403**, 398 (2000).

[28] R. Berman, *Thermal Conduction in Solids* (Clarendon Press, Oxford, 1976).

[29] Ashcroft and Mermin, *Solid State Physics* (Saunders College Publishing, Philadelphia, 1976).

[30] S. Legault, Ph.D. thesis, McGill University, 1999.

[31] C. Kittel, *Introduction to Solid State Physics, 4th edn* (John Wiley, New York, 1971).

[32] R. Berman, E. Foster, and J. Ziman, Proc. Roy. Soc. A **231**, 130 (1986).

[33] P. Klemens, Proc. Roy. Soc. (London) **A68**, 1113 (1955).

[34] R. Peierls, Annln. Phys. **3**, 1055 (1929).

[35] J. Callaway, Phys. Rev. **113**, 1046 (1959).

[36] C. Herring, Phys. Rev. **95**, 954 (1954).

[37] P. Kalugin, A. Chernikov, A. Bianchi, and H. Ott, Phys. Rev. B **53**, 21 (1996).

[38] B. Geilikman, Sov. Phys. –JETP **37**, 635 (1960).

[39] C. Caroli, P.-G. de Gennes, and J. Matricon, Phys. Rev. Lett. **9**, 307 (1964).

[40] N. Hayashi, T. Isoshima, M. Ichioka, and K. Machida, Phys. Rev. Lett. **80**, 2921 (1998).

[41] B. Pöttinger and U. Klein, Phys. Rev. Lett. **70**, 2806 (1993).

[42] Z. Tesanovič and P. Sacramento, Phys. Rev. Lett. **80**, 1521 (1998).

[43] M. Ichioka, A. Hasegawa, and K. Machida, Phys. Rev. B **59**, 184 (1999).

[44] M. Ichioka, A. Hasegawa, and K. Machida, Phys. Rev. B **59**, 1902 (1999).

[45] R. Cleary, Phys. Rev. **1**, 169 (1970).

[46] P. Ossi, *Disordered Materials. An introduction.* (Springer, Berlin, 2003).

[47] M. Dikeakos, Ph.D. thesis, McGill University, 2001.

[48] D. Turnbull, COntemporary Physics **10**, 473 (1969).

[49] C. Applegate and J. Bass, *Solid State Physics Source Book* (McGraw-Hill, New York, 1988).

[50] P. Duwez and R. Willens, Transactions of the Metallurgical Society of AIME **227**, 362 (1963).

[51] P. Duwez, Transactions of the American Society of Metals **60**, 607 (1967).

[52] N. Kovalenko, Y. Krasny, and U. Krey, *Physics of Amorphous Metals* (Wiley-Vch, Berlin, 2001).

[53] R. Zeller and R. Pohl, Phys. Rev. B **4**, 2029 (1971).

[54] W. Phillips *et al.*, *Amorphous Solids, Low-Temperature Properties* (Springer-Verlag, Berlin, 1981).

[55] S. Elliot, *Physics of Amorphous Materials* (Longman Scientific & Technical, New York, 1983).

[56] J. Graebner *et al.*, Phys. Rev. Lett. **39**, 1480 (1977).

[57] M. Higgins and S. Bhattacharya, Physica (Amsterdam) **257C**, 232 (1996).

[58] E. Rosemblum, S. Autler, and K. Gooen, Rev. Mod. Phys. **36**, 77 (1964).

[59] A. Troyanovsky *et al.*, Phys. Rev. Lett. **80**, 147006 (2002).

[60] P. Gammel *et al.*, Phys. Rev. Lett. **80**, 833 (1998).

[61] Y. Fasano *et al.*, Phys. Rev. B **66**, 020512 (2002).

[62] T. Berlincourt, R. Hake, and D. Leslie, Phys. Rev. Lett. **6**, 671 (1961).

[63] P. Kes and C. Tsuei, Phys. Rev. B **28**, 5126 (1983).

[64] J. Geers *et al.*, Phys. Rev. B **63**, 094511 (2001).

[65] R. Wördenber, P. Kes, and C. Tsuei, Phys. Rev. B **33**, 3172 (1986).

[66] M. Trudeau, Ph.D. thesis, Université de Montréal, 1986.

[67] F. Pobell, *Matter and Methods at Low Temperatures, 2nd ed.* (Springer-Verlag, Berlin, 1996).

[68] G. White, *Experimental techniques in Low temperature Physics* (Clarendon Press, Oxford, 1968).

[69] B. Lussier, Ph.D. thesis, McGill University, 1966.

[70] P. Lambert, Master's thesis, McGill University, 1998.

[71] R. van den Berg, S. Grondey, J. Kästner, and L. H. v., Solid State Comm. **47**, 137 (1983).